A novel Single Alpha-Helix-DNA-binding domain in CAF-1 promotes gene silencing and DNA damage survival through tetrasome-length DNA selectivity and spacer function

Ruben Rosas[1,5], Rhiannon R. Aguilar[2,3,5], Nina Arslanovic[2], Jessica K. Tyler[2,*] and Mair E. A. Churchill[1,4,*]

1. Program in Structural Biology and Biochemistry, University of Colorado School of Medicine, Aurora, CO 80045, USA.
2. Department of Pathology and Laboratory Medicine, Weill Cornell Medicine, New York, NY 10065, USA.
3. Weill Cornell/Rockefeller/Sloan-Kettering Tri-Institutional MD-PhD Program, New York, NY ,10065, USA
4. Department of Pharmacology, University of Colorado School of Medicine, Aurora, CO 80045, USA.
5. These authors contributed equally to this work.

*Correspondence: mair.churchill@cuanschutz.edu (M.E.A.C), jet2021@med.cornell.edu (J.K.T)
Department of Pharmacology and the Program in Structural Biology and Biochemistry
University of Colorado School of Medicine, Aurora, CO 80045, USA
Tel: 303-724-3670; FAX: 303-724-3663

Abstract

The histone chaperone chromatin assembly factor 1 (CAF-1) deposits nascent histone H3/H4 dimers onto newly replicated DNA forming the central core of the nucleosome known as the tetrasome. How CAF-1 ensures there is sufficient space for the assembly of tetrasomes remains unknown. Structural and biophysical characterization of the lysine/glutamic acid/arginine-rich (KER) region of CAF-1 revealed a 128 Å single alpha helix (SAH) motif with unprecedented DNA binding properties. Distinct KER sequence features and length of the SAH drive the selectivity of CAF-1 for tetrasome-length DNA and facilitate function in budding yeast. *In vivo*, the KER cooperates with the DNA-binding winged helix domain in CAF-1 to overcome DNA damage sensitivity and maintain silencing of gene expression. We propose that the KER SAH links functional domains within CAF-1 with structural precision, acting as a DNA binding spacer element during chromatin assembly.

Introduction

In eukaryotes, dynamic local and global chromatin structures regulate accessibility to the genome for all DNA dependent processes(Yadav, Quivy, and Almouzni, 2018; Klemm, Shipony, and Greenleaf, 2019). The nucleosome is the fundamental unit of chromatin, comprising two H3/H4 and two H2A/H2B histone dimers wrapped by approximately 147 bp of DNA(Luger et al., 1997). DNA replication requires the disassembly of parental nucleosomes, followed by a highly-regulated dynamic assembly process for recycling of parental histones and depositing nascent histones onto the newly replicated DNA(Smith and Stillman, 1991; Escobar, Loyola, and Reinberg, 2021). The histone chaperone chromatin assembly factor 1 (CAF-1) facilitates the dimerization of nascent H3/H4 dimers onto replicated DNA, forming the subnucleosomal structure known as the tetrasome(Smith and Stillman, 1989; Kaufman et al., 1995; Mattiroli et al., 2017a; Sauer et al., 2017; Sauer et al., 2018).

In multicellular organisms, the essential functions of CAF-1 are required for the maintenance of epigenetic landscapes and gene expression patterns(Cheloufi et al., 2015; Cheloufi and Hochedlinger, 2017; Smith and Whitehouse, 2012; Ramachandran and Henikoff, 2016; Sauer et al., 2018). How CAF-1 deposits H3/H4 at sites of DNA synthesis remains largely unknown. However, the identification of functional domains within CAF-1 has provided significant insight. Three subunits: Cac1, Cac2 and Cac3, form the CAF-1 complex(Sauer et al., 2018; Smith and Stillman, 1989). Central to the localization of CAF-1 to replicated DNA are interactions with the replisome through PCNA interacting peptides (PIP box) in the Cac1 subunit(Shibahara and Stillman, 1999; Krawitz, Kama, and Kaufman, 2002). Additionally, the DNA binding function of the Winged Helix Domain (WHD) located in Cac1 contributes to the recruitment of CAF-1 to sites of replication(Sauer et al., 2017; Zhang et al., 2016; Mattiroli et al., 2017b).

DNA binding studies of the *Saccharomyces cerevisiae* CAF-1 (yCAF-1) revealed a preference for binding to DNA that is at least 40 bp long(Sauer et al., 2017), which is slightly less

than the length of DNA needed to form a tetrasome(Luger et al., 1997; Donham, Scorgie, and Churchill, 2011). As the WHD binds to short (10-16 bp) DNA fragments(Zhang et al., 2016; Mattiroli et al., 2017b), it is unlikely to confer this DNA length dependence to CAF-1 or allow for sufficient spacing for the assembly of tetrasomes *in vivo*. However, the lysine/glutamic acid/arginine-rich (KER) region of the Cac1 subunit has been implicated as a possible second DNA-binding domain, as CAF-1 lacking the WHD could still bind to DNA(Sauer et al., 2017). Whether the KER cooperates with the WHD or PIP box to recruit CAF-1 to sites of DNA synthesis, contributes to the length-dependent DNA recognition of CAF-1, or has other biological roles remains unclear.

Here, we characterized the KER region of yCAF-1 using biophysical, structural, and functional approaches *in vitro* and in budding yeast. The crystal structure of the KER and DNA binding experiments revealed a novel single alpha helix (SAH) domain with DNA binding ability that we found drives the selectivity of yCAF-1 for tetrasome-length DNA. Features of the structure and sequence of the KER SAH required for DNA binding were defined. In yeast, the KER structure is important for CAF-1 mediated chromatin assembly through cooperation with the WHD during DNA damage repair and gene silencing.

Results

The KER is a major DNA binding domain in CAF-1 that cooperates with the WHD *in vivo.*

The previously observed DNA length preference of yCAF-1 (Sauer et al., 2017) cannot be explained by the DNA-binding properties of the WHD (Zhang et al., 2016; Mattiroli et al., 2017a; Sauer et al., 2017). To determine whether the KER promotes this DNA length preference, we first expressed and purified recombinant tri-subunit yCAF-1, KER (Cac1 residues 136–225, yKER), and WHD (Cac1 residues 457–606, yWHD) (Figure 1a and Figure 1-figure supplement 1a-c). Using electrophoretic mobility shift assays (EMSA) we measured the binding affinity for each protein to DNA fragments of different lengths (Figure 1b-i and Figure 1-figure supplement 2a,b). To determine the DNA binding affinities, the EMSA images were quantitated and the resulting binding curves fitted with Equation 1 (see Methods) (Figure 1j,k and Figure 1-figure supplement 2c), which gave values for the dissociation constant (K_D) and cooperativity (Hill coefficient, h) (Figure 1l). yCAF-1 and the isolated domains bound to DNA with the appearance of a ladder of bands, especially for the yKER that has the largest number of bands, which are related to the length of the DNA fragment (20, 30, 40 and 80 bp). These results indicate that multiple proteins bind to a single DNA fragment (Figure 1f-i) and the Hill coefficients suggest a cooperative mode of DNA binding (Figure 1l). For DNA of the same length (Figure 1l), the yKER had K_D values between 18 to 50 nM, whereas the yWHD bound 3 to 6 times more weakly. yCAF-1 had K_D values between those observed for the yKER and the yWHD, except for weaker binding to the 30 bp DNA fragment (K_D of 330 nM) (Figure 1l). This analysis shows that yCAF-1 has a higher affinity for DNA fragments in the range of 50-80 bp, which are DNA lengths considered to be sufficient for tetrasome formation (Donham, Scorgie, and Churchill, 2011). In contrast, increasing DNA length only slightly decreased K_D values for the yKER or yWHD (Figure 1l).

To determine the importance of the KER to the DNA binding function of yCAF-1, yCAF-1 lacking only the KER, Cac1 residues 136–225 (yCAF1 ΔKER), was produced (Figure 1-figure

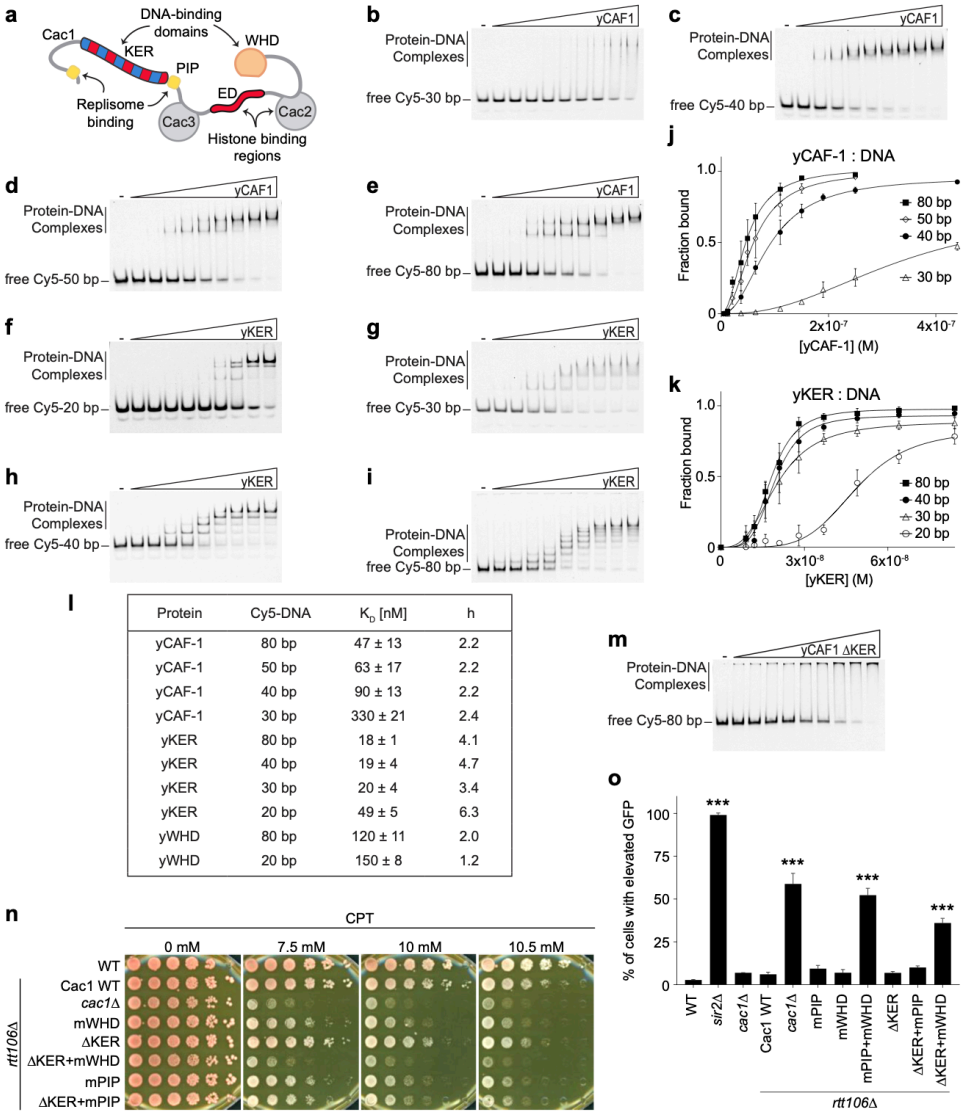

l

Protein	Cy5-DNA	K_D [nM]	h
yCAF-1	80 bp	47 ± 13	2.2
yCAF-1	50 bp	63 ± 17	2.2
yCAF-1	40 bp	90 ± 13	2.2
yCAF-1	30 bp	330 ± 21	2.4
yKER	80 bp	18 ± 1	4.1
yKER	40 bp	19 ± 4	4.7
yKER	30 bp	20 ± 4	3.4
yKER	20 bp	49 ± 5	6.3
yWHD	80 bp	120 ± 11	2.0
yWHD	20 bp	150 ± 8	1.2

Figure 1. The yKER region favors binding to tetrasome-length DNA and facilitates the function of yCAF-1 *in vivo*. a, Cartoon representing the molecular architecture of the yCAF-1 complex highlighting the protein subunits and functional domains. Domains include the K/E/R-rich (DNA-binding domain), PCNA interacting peptides (PIP boxes), Cac3 binding site (small), E/D-rich regions (histone binding), Cac2 binding site (Middle), and a DNA-binding winged helix domain (WHD). **b-i,** Representative images of EMSA experiments for yCAF-1 or yKER, with 2 or 3 nM of Cy5-DNA; the range of protein concentrations are: 5–250 nM and 9–84 nM, respectively. **j.k,** Quantitative analyses of all EMSAs of yCAF-1 or yKER with Cy5-labeled DNA. Data from at least three independent experiments were plotted as the mean and standard deviation (error bars). The binding curves were fitted using Eqn. 1. **l,** Table summarizing the dissociation constant (K_D) and Hill coefficient (h) values obtained from EMSAs of the indicated proteins and DNA. Values were obtained from fitting plots using Eqn. 1. **m,** Representative image of an EMSA experiment for yCAF-1 ΔKER with 3 nM of Cy5-80 bp DNA; the range of protein concentrations is 49–440 nM. **n,** Yeast spot assay with 5-fold serial dilutions of cultures of the indicated strains; grown in the presence of CPT at the specified concentrations. **o,** Bar graph indicating the percentage of cells exhibiting elevated GFP levels from yeast cultures of the indicated strains sorted by flow cytometry. Error bars indicate the standard deviation of the calculated values from three measurements. Statistical significance was calculated by Student's *t*-test where * = p<0.05, ** = p<0.01, and *** = p<0.001 relative to Cac1 WT cells. See also Figure 1 - Source data 1 and Source data 2.

supplement 1a) and tested using EMSA. Deletion of the KER region impaired DNA binding of yCAF-1 and also resulted in the failure of the complexes to migrate into the gel, possibly due to aggregation (Figure 1m). As the yCAF-1 ΔKER mutant still has the WHD, this residual DNA binding function might be due to the WHD or other unknown DNA-binding regions within CAF-1. Together, these data show that the KER binds more tightly to DNA than the WHD and the presence of the KER in the context of yCAF-1 is needed for high DNA-binding affinity.

As the KER confers the majority of DNA binding affinity to yCAF-1 *in vitro*, we investigated the impact of deleting the KER on CAF-1 function in chromatin assembly after DNA replication and repair(Smith and Stillman, 1991; Ye et al., 2003; Smith and Stillman, 1989; Gaillard et al., 1996; Mello et al., 2002; Tyler et al., 1999). Yeast cells harboring defective CAF-1, including loss of the Cac1 subunit, or loss of its WHD, PIP box, or histone binding regions (Figure 1a), have been shown to be more sensitive to DNA damaging agents and have impaired establishment of chromatin landscapes (Li et al., 2008b; Zhang et al., 2016). We examined cell growth and survival of budding yeast mutants in a spot assay in the presence of the DNA topoisomerase I inhibitor Camptothecin (CPT) (Eng et al., 1988) and Zeocin. While CPT stabilizes covalently bound DNA topoisomerase I complexes on chromatin resulting in replication fork collisions and DNA double-strand breaks (DSBs) (Pommier, 2006), Zeocin intercalates into DNA to induce DSBs independent of the replication process (Chankova et al., 2007). yCAF-1 mutants were generated by site-directed mutagenesis of the gene that encodes the Cac1 subunit (*CAC1)* via CRISPR-Cas9 at the endogenous genomic locus in yeast strains deleted for the *RTT106* gene (*rtt106*Δ) that encodes for a histone chaperone with overlapping roles of CAF-1 in yeast (Huang et al., 2005; Li et al., 2008a) (Figure 1-figure supplement 1d). Deletion of Cac1 residues 136–225 that encode for the KER region (ΔKER) resulted in a mild sensitivity to CPT and Zeocin (Figure 1n and Figure 1-figure supplement 2d). Inhibition of the DNA binding function of the WHD through point mutations in Cac1 residues K564E/K568E (mWHD) in yeast (Zhang et al., 2016) showed higher sensitivity to CPT and Zeocin than the deletion of the KER. Strikingly, the double mutant

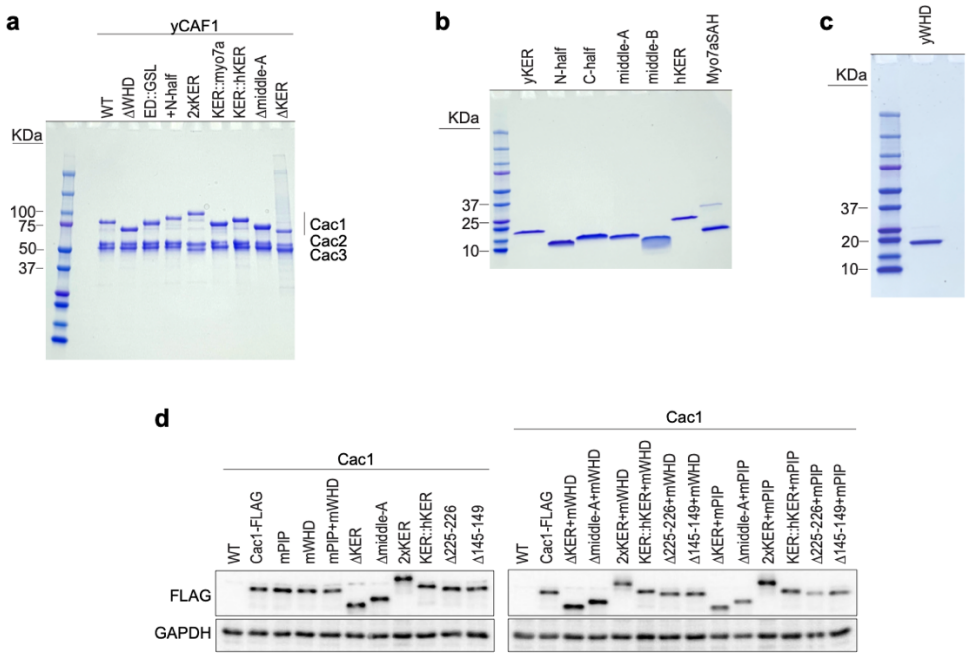

Figure 1-figure supplement 1. Quality of proteins used in this study. **a-c,** 4-20 % gradient SDS-PAGE stained with Coomassie Blue of the indicated purified protein domains (**b and c**) or yCAF-1 complexes (**a**). **d,** Western Blot of yeast cell lysates harboring the indicated Cac1 mutations along with a FLAG tag motif incorporated at the C-terminus of Cac1. An anti-FLAG antibody was used to detect expression of the FLAG-tagged Cac1 proteins from cell lysates. An anti-GAPDH antibody was used to determine the levels of GAPDH protein from the cell lysates as a loading control. See also Figure 1 - figure supplement 1 - Source data 1.

ΔKER+mWHD showed higher CPT and Zeocin sensitivity than either mutant alone, and to a similar extent observed when the Cac1 subunit is absent (*cac1*Δ) (Figure 1n, Table 1 and Figure 1-figure supplement 2d). These results are consistent with roles for both the KER and WHD in CAF-1 function because at least one DNA-binding domain appears to be sufficient to maintain some CAF-1 function *in vivo* and overcome repercussions of DSBs, both dependent and independent of DNA replication.

We also investigated a potential coordinated role between the KER and the PIP box for the recruitment of CAF-1 to the replisome. Inhibition of the PIP box downstream of the KER (Figure 1a) by substitution of Cac1 residues F233A/F234A (mPIP) (Zhang et al., 2016) did not result in an increase in sensitivity to CPT and Zeocin when in combination with ΔKER (ΔKER+mPIP) (Figure 1n, Table 1 and Figure 1-figure supplement 2e). This is in contrast to mWHD+mPIP cells (Table 1 and Figure 1-figure supplement 2e) where WHD and the PIP box cooperate in their recruitment function (Zhang et al., 2016). These results suggest a role of the KER independent of recruitment of CAF-1 to the replisome via the PIP box.

CAF-1 function can influence cellular gene expression profiles, presumably by the deposition of nascent nucleosomes that promote the reestablishment of chromatin landscapes post-DNA replication (Ramachandran and Henikoff, 2016). To investigate the role of the KER in this process, we used strains with a Green Fluorescent Protein (GFP) reporter in the *HMR* mating-type locus of budding yeast. In normal conditions the *HMR* locus is silenced but defects in the chromatin result in expression of GFP with measurable fluorescence by flow cytometry (Huang et al., 2005; Laney and Hochstrasser, 2003) (Figure 1o and Figure 1-figure supplement 2f).

Functionality of this reporter assay was confirmed by deletion of *SIR2* (*sir2*Δ), a subunit of the silent information regulator (SIR) complex required for the establishment of silencing of the *HMR* locus (Rine and Herskowitz, 1987). Almost 100% of *sir2*Δ cells exhibited GFP fluorescence (Figure 1o). Consistent with the CPT and Zeocin sensitivity assays, we found that ΔKER, mWHD, and mPIP cells had low expression of GFP. As previously reported, a high percentage of

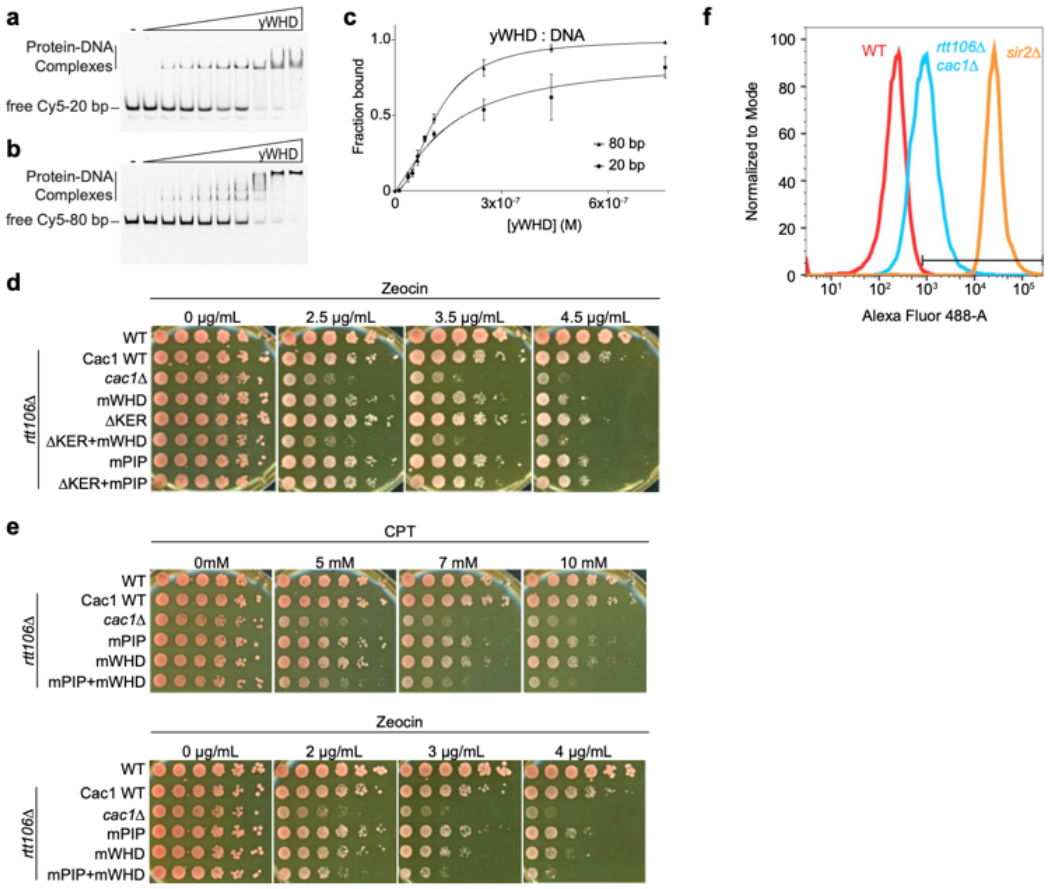

Figure 1-figure supplement 2. CAF-1 DNA binding analysis and *in vivo* assays. a,b, Representative images of EMSAs with 2 nM of the indicated Cy5-labeled DNA and yWHD over a range of protein concentrations of 12–760 nM. **c,** Quantitative analyses of EMSAs of yWHD with Cy5-labeled DNA. Data from at least three independent experiments were plotted as the mean and standard deviation (error bars). The binding curves were fitted using Eqn. 1. **d,e,** Yeast spot assay with 5-fold serial dilutions of cultures of the indicated strains; grown under in the presence of CPT, or Zeocin at the specified concentrations. **f,** Representative flow cytometry histograms of cultures of the indicated yeast strains sorted with the Alexa Fluor 488-4 channel that detects GFP signal. See also Figure 1 - figure supplement 2 - Source data 1.

192 **Table 1**. Relative sensitivity to CPT and Zeocin of yeast cells harboring CAF-1 mutations in a
193 *rtt106*Δ background.
194
195

	CPT sensitivity	**Zeocin sensitivity**
Cac1 WT	+	+
*cac1*Δ	+++++	+++++
ΔKER	++	++
mWHD	+++	+++
mPIP	+++	++
mWHD+mPIP	+++++	+++++
ΔKER+mWHD	+++++	+++++
ΔKER+mPIP	+++	++
Δmiddle-A	++	++
Δmiddle-A+mWHD	+++++	+++++
2xKER	++	+++
2xKER+mWHD	++	+++
Δ145-149	+	+
Δ145-149+mWHD	++++	+++++
Δ225-226	++	++
Δ225-226+mWHD	+++++	+++++
Δ225-226+mPIP	+++	+++
KER::hKER	+	++
KER::hKER+mWHD	++++	+++++

196 *cac1Δrtt106Δ* cells have increased GFP expression and mPIP+mWHD cells have a comparable
197 level of GFP expression, suggesting a near-total loss of CAF-1 function (Zhang et al., 2016). No
198 increase in GFP expression is seen in response to combined ΔKER+mPIP cells when compared
199 to mPIP alone (Figure 1o). In contrast, ΔKER+mWHD cells had GFP expression, similar to
200 *cac1Δrtt106Δ* cells, suggesting a near-complete loss of CAF-1 function. Together, these results
201 suggest that yCAF-1 requires the coordinated action of the KER and WHD to prevent DNA
202 damage sensitivity and establish silencing of repressed genes *in vivo*. Since both the KER and
203 the WHD bind to DNA, they might have overlapping yet complementary functions in targeting or
204 aligning CAF-1 correctly to the DNA during nucleosome assembly.
205
206 **The KER is a first-in-class single alpha helix (SAH) DNA-binding domain.**
207 To gain insight into how the KER region binds to DNA and facilitates CAF-1 function *in vivo*,
208 we determined the structure of the yKER at 2.81 Å resolution. Crystals grown of a maltose binding
209 protein (MBP)-KER fusion construct (Figure 2a, Figure 2-figure supplement 1a,b and
210 Supplementary Table 4) contained four copies of the MBP-yKER per asymmetric unit. The yKER
211 extended from the MBP as an almost entirely solvent exposed continuous alpha helix (Figure 2-
212 figure supplement. 1b). The longest yKER helix modeled (PDB 8DEI; molecule A) is 128 Å long
213 with 23 helical turns, encompassing Cac1 amino acids 136–221 (Figure 2a). Superposition of the
214 four KER copies gives root mean square deviation (R.M.S.D.) values between 0.66 and 2.2 Å, as
215 the helices have a marked curvature in the region of aa 165-190 and larger deviations at the
216 termini (Figure 2-figure supplement 1c). In the structure, we saw no evidence of interactions
217 between yKER helices or formation of any tertiary structure, consistent with the definition of a
218 single alpha helix (SAH) domain (Wolny et al., 2017). Inspection of the sequence of the yKER
219 reveals a pattern of opposite-charged residues, lysine/arginine and glutamic acid, that are 3 or 4
220 residues apart (Figure 2b), capable of forming an ion pair network. Such a network confers

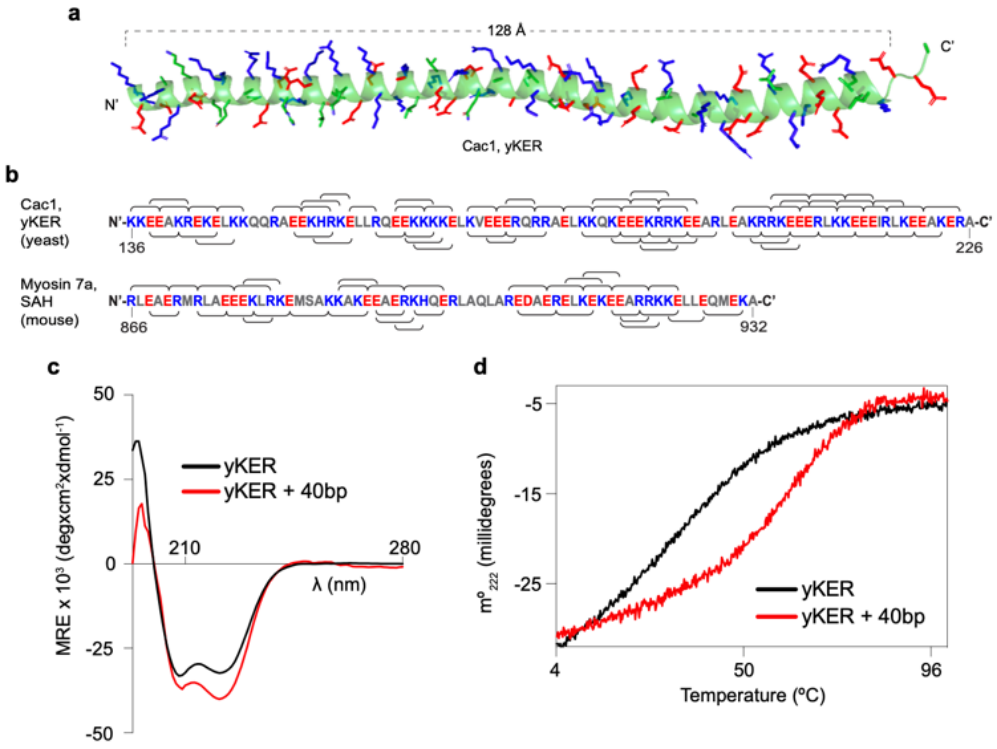

Figure 2. The yKER is a single alpha-helix (SAH) domain that forms a stable complex with DNA. a, Ribbon representation of the X-ray crystal structure of yCAF-1 KER region. Cac1 residues 136–222 are shown with side chains of residues Lys, Arg, and His colored in blue and Glu in red. **b,** Schematic diagram of the indicated SAH sequences with positively charged residues Arg, Lys, and His, colored in blue; and negatively charged residue Glu and Asp colored in red. The brackets along the sequence represent predicted interhelical i, i+4 or i, i+3 ion pairs. **c,** Overlap of circular dichroism spectra of yKER alone and in the presence of 40 bp DNA. DNA signal was subtracted from the yKER + 40 bp DNA sample to observe only changes in the protein component. **d,** Thermal denaturation monitored by circular dichroism at 222 nm (m^{o}_{222}) of yKER alone and in the presence of 40 bp DNA. See also Figure 2 - Source data 1.

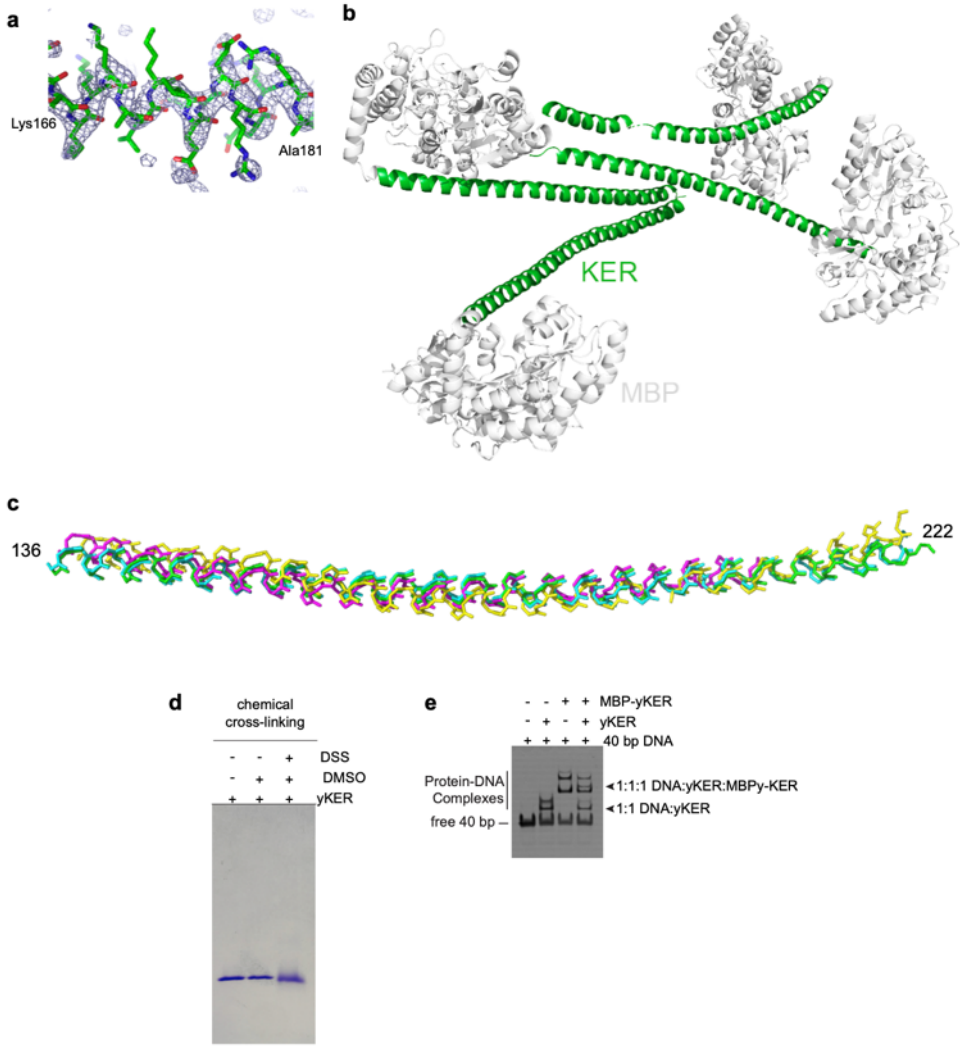

Figure 2-figure supplement 1. Analysis of the MBP-yKER crystal structure. a, Diagram showing electron density for a region of the yKER. The 2Fo-Fc composite omit map was contoured at 1 sigma. **b,** Crystal packing diagram showing the arrangement of the four molecules in the asymmetric unit. **c,** Diagram showing the superposition of the yKER domains from molecules A-D, colored green, cyan, magenta, and yellow, respectively. **d,** SDS-PAGE stained with Coomassie Blue showing chemical cross-linking of the yKER domain. The indicated lanes include the untreated yKER, yKER incubated with the vehicle (DMSO) and yKER crosslinked with disuccinimidyl suberate (DSS). The diffuse band indicates intra-polypeptide crosslinking. **e,** Representative image of a heterogenous subunit EMSA experiment with 40 bp DNA, the yKER and MBP-yKER. The proteins and DNA were mixed at a concentration of 900 nM in all reactions. The observed signal corresponds to Cy5-40 bp DNA that was spiked in all reactions to facilitate visualization. The interpreted composition of the protein-DNA complexes observed is indicated. See also Figure 2 - figure supplement 1 - Source data 1.

stability to the helix so that SAH domains can be completely solvent exposed in solution (Batchelor et al., 2019; Sivaramakrishnan et al., 2008; Wolny et al., 2017; Swanson and Sivaramakrishnan, 2014); such as in the well characterized Myosin7a SAH (Barnes et al., 2019). The circular dichroism (CD) spectrum of the KER showed characteristics of only alpha helical secondary structure, including the positive absorption band at 195 nm and two negative bands at 208 and 222 nm (Figure 2c), validating in solution the structure of the KER observed in the crystal. Interestingly, binding to DNA increased the alpha helical content of the yKER (Figure 2c) without changes in the CD signal from the DNA (Figure 2-figure supplement. 2a), suggesting that no major DNA structural changes occur.

Fundamental to the definition of SAH domains is that they exhibit non-cooperative denaturation transitions due to a lack of tertiary structure (Wolny et al., 2017; Wolny et al., 2014; Süveges et al., 2009). This behavior is also observed in the thermal denaturation monitored by CD at 222 nm of the yKER (Figure 2d). Furthermore, chemical crosslinking with disuccinimidyl suberate (DSS) showed no evidence of KER multimers (Figure 2-figure supplement. 1d), supporting the conclusion that the yKER does not form a tertiary structure. In contrast, in the presence of 40 bp DNA, the thermal denaturation of the yKER showed an increase of 10 °C in the melting temperature and a two-state cooperative unfolding transition (Figure 2d), which demonstrates the ability of the yKER to form a stably folded protein-DNA complex. The monomeric state of the yKER also suggests that the additional yKER-DNA complexes observed in the EMSAs (Figure 1f-i) are due to the addition of yKER monomers to the same molecule of DNA. This was substantiated through use of a heterogenous subunit EMSA (Hope and Struhl, 1987; Gangelhoff et al., 2009) with the yKER, MBP-yKER and a combination of the two proteins. The mixed-protein subunit:DNA complexes (Figure 2-figure supplement 1e) can only be explained if the KER forms no obligate oligomers on the DNA. Rather, multiple monomers of yKER are recruited to the same molecule of DNA, creating the multiplicity of bands in the EMSA. Finally, DNA binding has not been reported for other SAH domains even though they have a similar amino

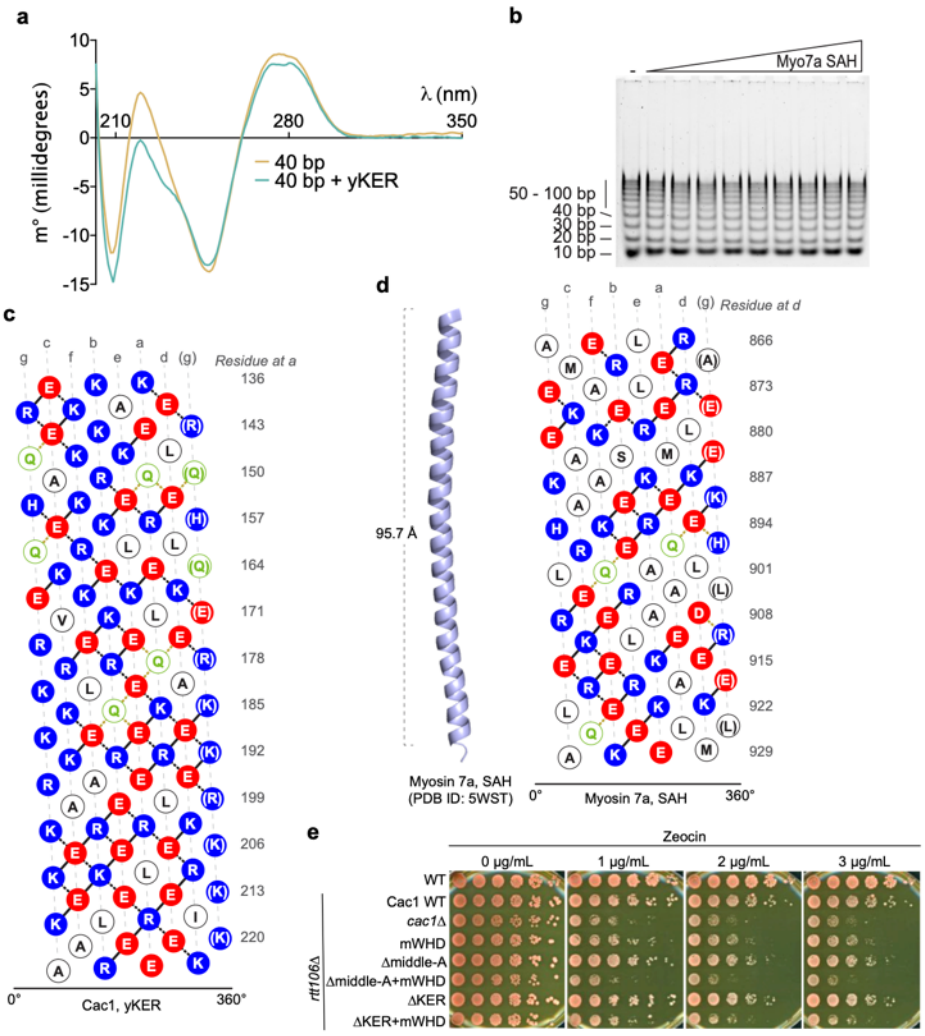

Figure 2-figure supplement 2. DNA binding properties of the yKER. a, Graph of circular dichroism spectra of 40 bp DNA alone and in the presence of yKER. The yKER spectrum was subtracted from the 40 bp + yKER sample to observe only changes in the DNA component. **b,** Representative image of a SYBR green-stained EMSA experiment for Myosin 7a SAH with a 10 bp DNA ladder. 500 nM of total DNA ladder was incubated with a range of 64 nM-1 µM concentrations of protein. **c,** Helical net diagram of yKER. In this representation, the SAH structure has been split along a helical track and unwound so it can be displayed in 2D. Amino acids colored in red are negatively charged, blue are positively charged, green is glutamine and white are other polar or hydrophobic. Lines connecting colored residues represent predicted ion pair interactions based on strength: solid lines, strong; black dashed lines, medium; yellow dashed lines, weak. **d,** Crystal structure of the Myosin 7a SAH along with its helical net representation as in **c**. **e,** Yeast spot assay with 5-fold serial dilutions of cultures of the indicated strains; grown in the presence of Zeocin at the specified concentrations. See also Figure 2 - figure supplement 2 - Source data 1.

acid composition (Figure 2b and Figure 2-figure supplement 2c,d). Examination of a purified Myosin7a SAH (Barnes et al., 2019) (Figure 1-figure supplement 1b and Figure 2-figure supplement 2b) using EMSA detected no DNA binding, indicating that the DNA binding properties of the yKER are not a general feature of SAH domains.

The yKER requires both the alpha helical structure and positively charged residues for DNA binding and yCAF-1 function *in vivo*.

As the yKER is a novel DNA-binding SAH, it was important to define which sequence features are responsible for the DNA binding functionality. We noticed that the yKER SAH is particularly enriched in positively charged residues, unlike the Myosin7a SAH (Figure 2-figure supplement 2c,d). These residues are biased towards one face of the yKER helix and confer a net positive charge along most of the length of the yKER, which is concentrated toward the N-terminal and middle regions (Figure 3a). To map the DNA binding region, we designed and purified five truncated versions of the yKER (Figure 3a and Figure 1-figure supplement 1b). These proteins exhibited different alpha helical content, which was markedly greater for the constructs containing C-terminal regions (Figure 3b). However, only the middle-A protein (residues 155-204) exhibited strong DNA binding similar to the intact KER (Figure 3a,c-g), whereas the N-half and middle-B constructs, which partially overlap with middle-A, did not bind well to DNA (Figure 3e,g). Although regions of the yKER outside of the middle-A region likely contribute to KER function, the middle-A region is required for DNA binding due to both the positively charged residues and alpha helical structure. Notably, deletion of the middle-A residues from yCAF-1 (yCAF1 ∆middle-A) abrogates binding of yCAF-1 to DNA (Figure 3h), confirming the importance of this region. Interestingly, we also observed that yCAF1 ∆middle-A binds to DNA worse than the deletion of the KER (yCAF1 ∆KER) (Figure 3h), suggesting that residual SAH structure might not support the correct organization or architecture of yCAF-1 in a manner that hinders the activity of the WHD. In the context of CAF-1, a substitution of the KER for the Myosin 7a SAH (KER::Myo7a) in

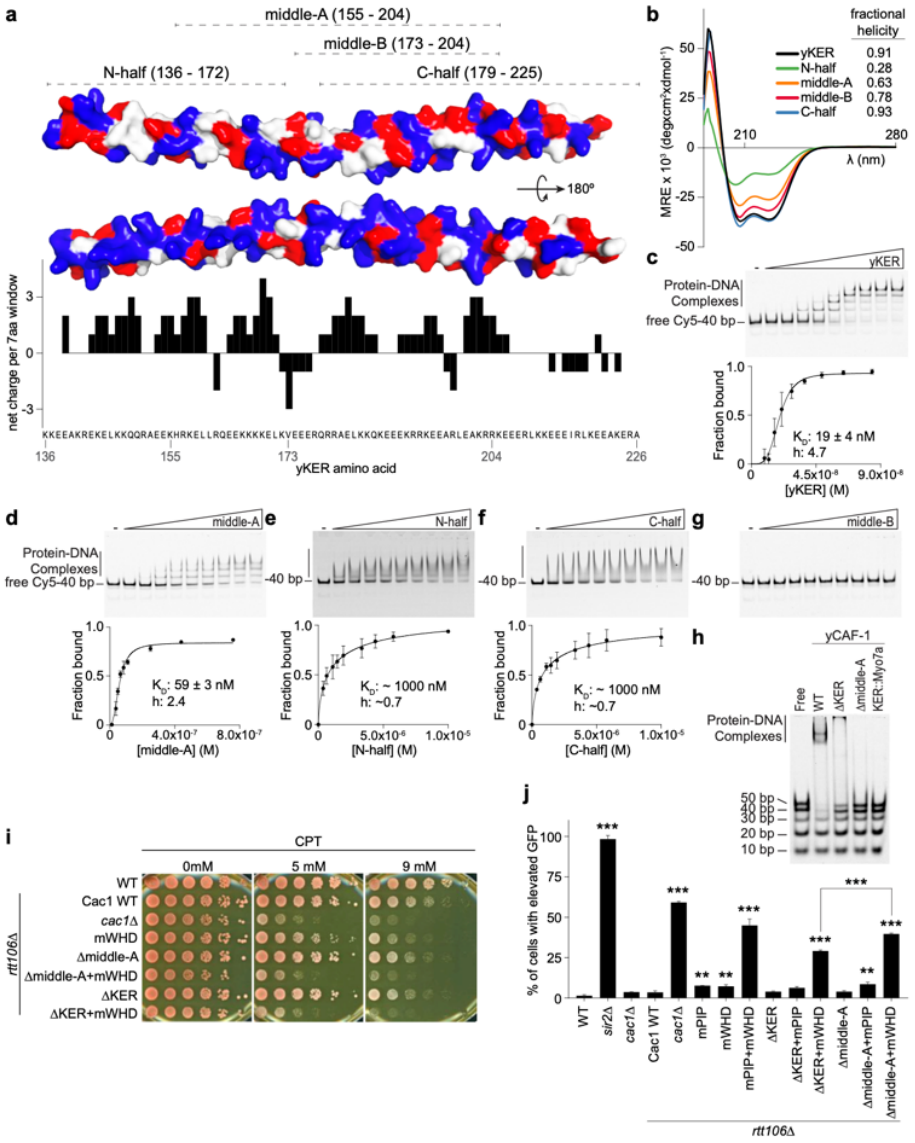

Figure 3. The yKER middle region is required for DNA binding and yCAF-1 function *in vivo*. a, Surface representation of two views of the yCAF-1 KER structure with basic residues colored in blue, acidic in red, and polar or hydrophobic in grey. The dashed lines at the top illustrate the yKER truncations under investigation. The bar graph represents the net charge calculated for a sliding window of 7 amino acids along the yKER sequence. The resulting net charge was assigned to the fourth residue in the window. **b,** Overlay of circular dichroism spectra of the yKER constructs indicated in **a**. **c-g,** Representative images of EMSA experiments and binding curves for the yKER constructs indicated in **a**. Cy5-40 bp DNA (either 2 or 2.5 nM) binding was observed over a range of protein concentrations of 9–84 nM for the yKER, 12–760 nM for the middle-A, 0.37–1 μM for N-half, C-half, and middle-B. K_D and h values were calculated from binding curves fitted with Eqn. 1 and were plotted as the mean of at least three independent experiments. **h,** Representative image of an EMSA showing the binding of a fixed concentration (250 nM) of yCAF-1, yCAF-1 ΔKER, yCAF-1 Δmiddle-A, and yCAF-1 KER::Myo7aSAH proteins binding to a set of different length of Cy5-labeled DNA fragments at 1 nM each. **i,** Yeast spot assay with 5-fold serial dilutions of cultures of the indicated strains; grown in the presence of CPT at the specified concentrations. **j,** Bar graph indicating the percentage of cells exhibiting elevated GFP levels from yeast cultures of the indicated strains sorted by flow cytometry. Error bars indicate the standard deviation of the calculated values from three measurements. Statistical significance was calculated by Student's *t*-test where * = p<0.05, ** = p<0.01, and *** = p<0.001 relative to Cac1 WT cells. See also Figure 3 - Source data 1.

yCAF-1, also abolished DNA binding (Figure 3h). *In vivo*, ΔmiddleA yeast behave like the ΔKER cells, exhibiting similar sensitivity to CPT and Zeocin, and even higher GFP expression levels in the silencing assay when in combination with mWHD (Figure 3i,j, Table 1, and Figure 2-figure supplement 2e). Taken together, we conclude that a specific region within the KER domain (middle-A) simultaneously forms an alpha helix and engages with DNA to drive DNA binding and the biological functions of yCAF-1.

The KER confers the selectivity of CAF-1 for tetrasome-length DNA.

Consistent with previous results (Sauer et al., 2017), and in Figure 1, yCAF-1 was found to have the highest binding affinity for DNA fragments that are at least 40 bp in length, which suggests a DNA-length selective property of CAF-1 that is driven by the KER. To test this hypothesis, we developed a novel EMSA approach, which uses equimolar concentrations of Cy5-labeled DNA fragments spanning 10–50 bp in length (Cy5-DNA ladder) to detect the DNA length preferences of CAF-1 under competition conditions between different lengths of DNA (Figure 4a-e). The free DNA signal for each fragment in the Cy5-DNA ladder was quantitated and plotted as a function of protein concentration. Subjecting yCAF-1 to this assay resulted in a DNA-length selective binding behavior, as shown by the preferential depletion of the 50 and 40 bp DNA fragments from the free DNA at lower concentrations of yCAF-1 compared to the 20 and 30 bp fragments (Figure 4a), while 10 bp remained unchanged. In order to visualize these differences in competition, we plotted the protein concentration required to give half-maximal depletion as a means to compare different proteins and different DNA lengths in the assay (Figure 4f). We observed a threshold effect that yCAF-1 prefers to bind to DNA of at least 40 bp in length (Figure 4f). Similarly, the yKER bound to the Cy5-DNA ladder in a DNA-length dependent manner. However, the yKER substantially depleted 30 and 20 bp fragments from the free DNA at lower concentrations (Figure 4b), revealing a very slight threshold effect compared to yCAF1. In contrast, the yWHD exhibited virtually no DNA-length selective binding, except that like the KER, the

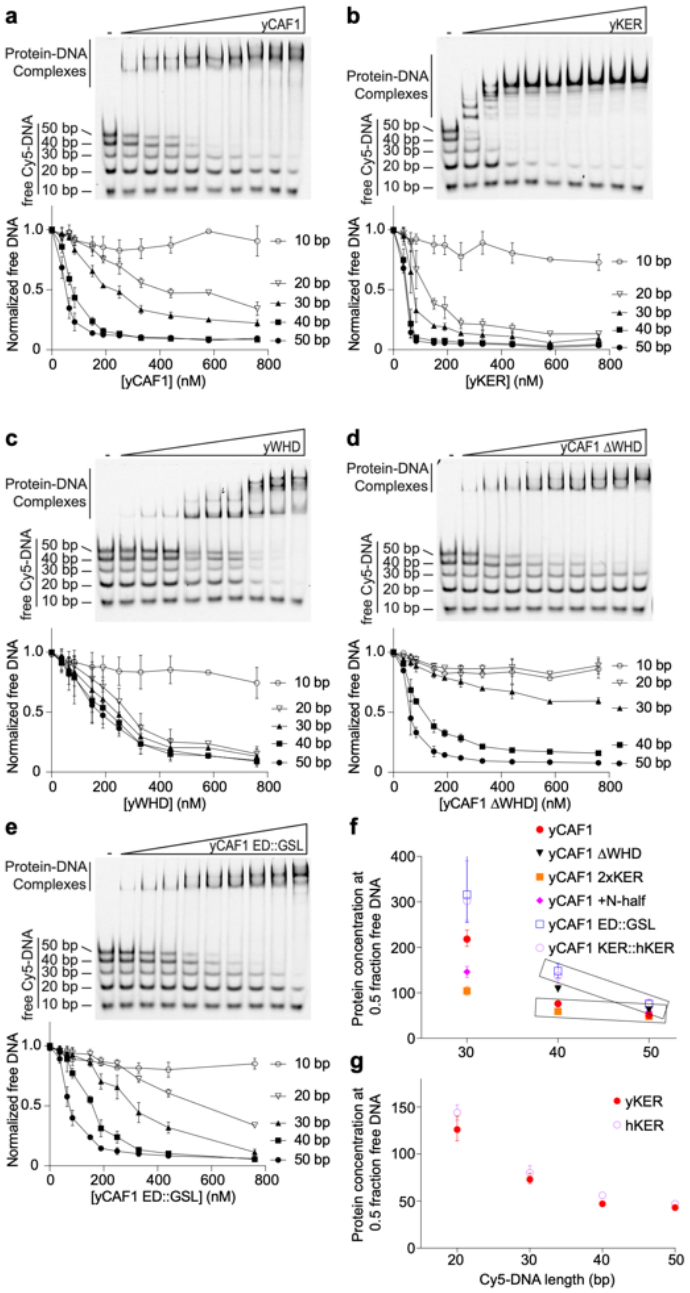

Figure 4. The yKER confers DNA-length selectivity to yCAF-1. a-e, Representative images of EMSAs showing DNA binding of yCAF-1, yKER, yWHD, yCAF-1 ΔWHD, or yCAF-1 ED::GSL where each Cy5-labeled DNA fragment is at 1 nM concentration and the range of protein concentration was 37–760 nM for all constructs. Below each gel image, the graph shows the quantitation of free (unbound) DNA signal for each Cy5-labeled DNA as a function of protein concentration. The data are plotted as the mean and standard deviation from at least three measurements. **f,g,** Plots representing the protein concentration required to achieve 50% depletion of the individual DNA fragments from the Cy5-DNA ladder for the indicated yCAF-1 constructs (**f**) or CAF-1 domains (**g**). See also Figure 4 - Source data 1.

shortest 10 bp DNA was bound poorly (Figure 4c). yCAF-1 with the WHD deleted (Cac1 amino acids 520–606) (yCAF1 ΔWHD) did not bind well to the 10-30 bp fragments, but did have a slight preference for the 50 bp over the 40 bp DNA (compare Figure 4a and d). Relevant to this observation, previous studies revealed that in a truncated form of CAF-1, the WHD interacts with the ED region (Figure 1a) and that H3/H4 dimer binding to the ED was needed to displace the WHD and free it to bind to DNA (Mattiroli et al., 2017b). This 'autoinhibited state' of the WHD can also be released through substitution of Cac1 residues 397–431 in the ED region by a glycine/serine/leucine linker (ED::GSL), which decreases the affinity of the WHD for the ED and allows the WHD to bind DNA in a histone-free manner (Mattiroli et al., 2017b). Therefore, we recapitulated the ED::GSL substitution in the context of full-length yCAF-1 (yCAF1 ED::GSL) (Figure 4e) and subjected it to the Cy5-DNA ladder assay. We found that yCAF1 ED::GSL showed a slight preference for the 50 bp DNA compared to the 40 bp (Figure 4e,f), suggesting that the uninhibited WHD contributes further to the length of DNA recognized by CAF-1. Together, these results demonstrate that the KER, but not the WHD, equips yCAF-1 with a DNA-length selectivity function that favors binding to DNA fragments that are at least 40 bp in length. Also, the presence of the WHD permits yCAF1 binding to 20 and 30 bp DNA, suggesting it has either a direct or indirect contribution to DNA binding of yCAF-1; and that there is a further contribution to the length threshold in the state where the WD is released from the ED.

The length of the KER alters CAF-1 DNA length recognition and modulates yCAF-1 functions *in vivo*.

The difference in DNA length selectivity between the KER in isolation compared to yCAF-1 (Figure 1l and Figure 4a,b) suggests that the context of the KER within the CAF-1 complex directs preferential binding to the longer DNA fragments. To investigate this, we made perturbations to the length of the KER in yCAF1 and evaluated the effects on DNA binding and function *in vivo*. We expressed and purified a yCAF-1 mutant that contains two KER domains in tandem (yCAF1

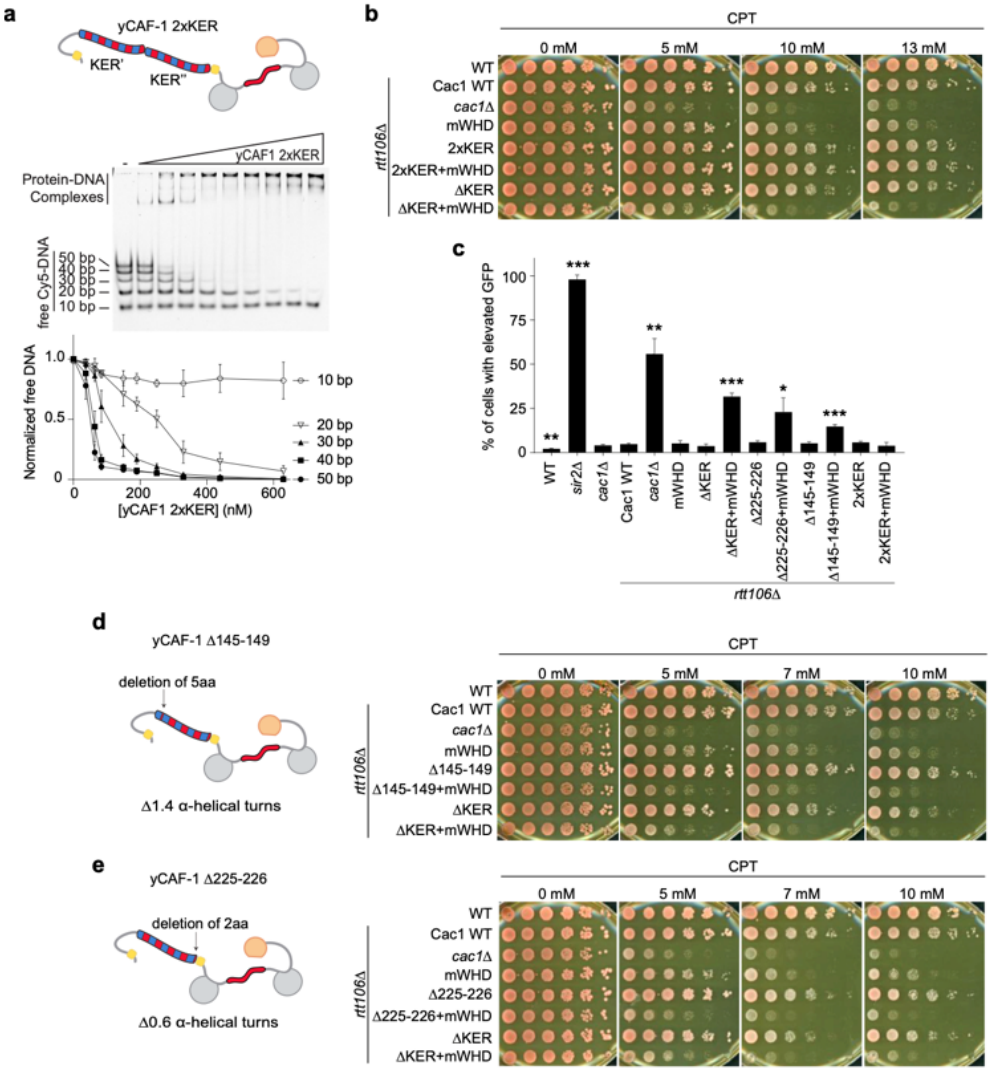

Figure 5. The length and the phase of the yKER SAH modulates yCAF-1 functions *in vivo*. **a,** Cartoon representing the yCAF-1 2xKER construct along with a representative image of an EMSA of showing binding to a set of Cy5-labeled DNA fragments (1 nM each) with a range of protein concentrations from 37 to 630 nM. Below the EMSA image, the free (unbound) DNA signal for each Cy5-labeled DNA is plotted as a function of the protein concentration. The error bars are the standard deviation from at least three measurements. **b,** Yeast spot assays with 5-fold serial dilutions of cultures of the indicated strains; grown in the presence of CPT at the specified concentrations. **c,** Bar graph indicating the percentage of cells exhibiting elevated GFP levels from yeast cultures of the indicated strains sorted by flow cytometry. Error bars indicate the standard deviation of the calculated values from three measurements. Statistical significance was calculated by Student's *t*-test where * = p<0.05, ** = p<0.01, and *** = p<0.001 relative to Cac1 WT cells. **d,e,** Yeast spot assays as in **b**, where cartoons on the left represent the shift of alpha-helical turns for the indicated KER deletions in yCAF-1. See also Figure 5 - Source data 1.

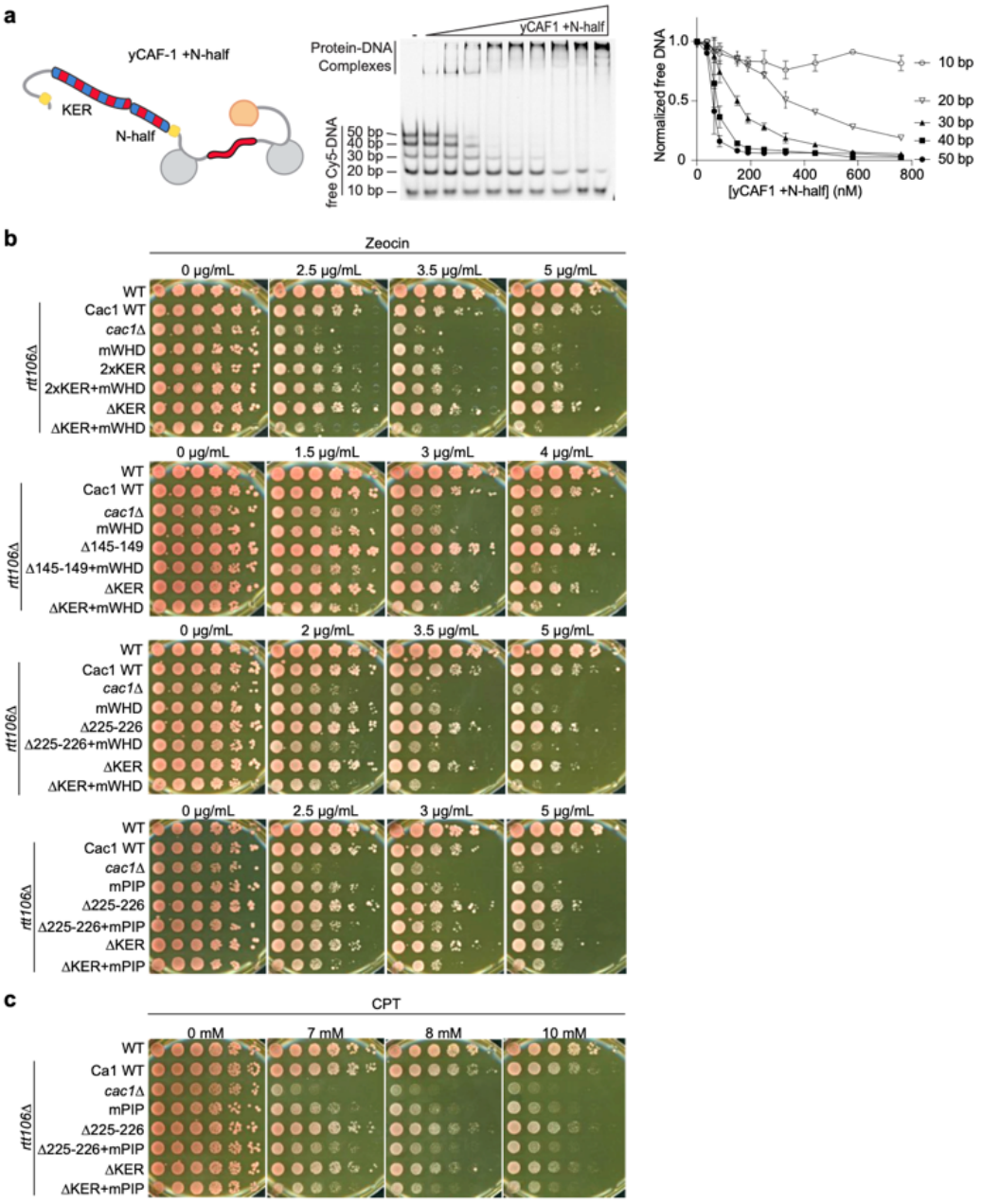

Figure 5-figure supplement 1. Analysis of the yKER length. a, Representative image of and EMSA experiment of yCAF-1 +N-half, where each Cy5-labeled DNA fragment was at 1 nM concentration and the range of protein concentration was 37–760 nM. The graph shows the quantitation of free (unbound) DNA signal for each Cy5-labeled DNA as a function of protein concentration. **b,c,** Yeast spot assay with 5-fold serial dilutions of cultures of the indicated strains; grown in the presence of Zeocin or CPT at the specified concentrations. See also Figure 5 - figure supplement 1 - Source data 1.

2xKER) by introducing an additional yKER (amino acids 136–225) in the Cac1 subunit immediately after the endogenous 225 residue (Figure 1-figure supplement 1a). Examination of yCAF1 2xKER in our Cy5-DNA ladder experiment showed that unexpectedly the additional KER did not alter the DNA-length threshold of 40 bp (Figure 5a, 4f). A similar result was observed with a yCAF-1 mutant that contains an additional KER N-terminal half of the KER (Cac1 residues 136–172) added after the endogenous 225 residue of Cac1 (yCAF1 +N-half) (Figure 4f and Figure 5-figure supplement 1a). *In vivo*, yCAF1 2xKER (2xKER) exhibited mild sensitivity to CPT (Figure 5b) and Zeocin (Figure 5-figure supplement 1b) to a similar extent as seen for ΔKER cells. Surprisingly, 2xKER in combination with inhibition of the WHD (2xKER+mWHD) did not have an additive effect unlike ΔKER in both CPT and Zeocin conditions (Figure 5b and Figure 5-figure supplement. 1b). Likewise, the 2xKER mutant caused no significant loss of silencing in yeast and it did not increase this effect when in combination with mWHD (Figure 5c). Together, addition of a KER sequence did not result in substantial differences in the DNA-length selectivity of yCAF-1, and did not impact the ability to overcome DNA damage and maintain gene silencing *in vivo*.

We then explored whether truncations of the KER helix have an effect in CAF-1 function *in vivo*. We made a short deletion within the basic region of the KER (Δ145-149) (Figure 3a), which removes 5 amino acid residues, shortens the helix by 1.4 turns and changes the phase of the helix. The deletion is not in the main DNA binding region of the KER (Figure 3) and is not expected to alter the DNA binding function of the KER. Interestingly, Δ145-149 cells behave like ΔKER cells, exhibiting similar sensitivity to CPT and Zeocin, as well as high GFP expression levels in our silencing assay when in combination with mWHD (Figure 5c,d, Table 1, and Figure 5-figure supplement. 1b). Strikingly, identical results were found when only the deletion of the last two C terminal residues 225-226 (Δ225-226) of the KER region in the Cac1 subunit were made (Figure 5e,c, Table 1 and Figure 5-figure supplement. 1b,c). We conclude that a very specific length of the yKER is critical to overcome DNA damage and maintain gene silencing *in vivo*.

The longer human KER alters DNA-length dependent binding and does not substitute for the yKER in yCAF-1 *in vivo*.

Our results from altering the length of the KER of CAF-1 in yeast revealed that CAF-1 function is highly sensitive to the length or phase of the helix, where the deletion of only two residues was sufficient to impair yCAF-1 function similar to a complete deletion of the KER (Figure 5). The length of the KER regions in other species differ. In the human homologue CHAF1A, the KER has a similar distribution of basic residues, but it is at least 20 residues longer than the yKER (Figure 6a). To address the hypothesis that the longer hKER might have different DNA binding properties than the yKER, we expressed and purified the hKER (CHAF1A residues 331–441) and using CD found that it has high alpha helical content, and exhibits non-cooperative unfolding as expected for a SAH (Figure 1-figure supplement 1b and Figure 6-figure supplement 1a-c). Subjecting the hKER to our Cy5-DNA ladder assay resulted in identical DNA-length selectivity behavior to the yKER (Figure 6b compared to 4b). However, substitution of the yKER for the hKER in yCAF-1(yCAF1 KER::hKER) (Figure 1-figure supplement 1a) slightly altered the DNA-length selectivity function of yCAF-1, as seen by the slight difference between the depletion of the 50 bp DNA fragments relative to the shorter DNA in our Cy5-DNA ladder assay (Figure 6c compared to 4a). This difference is largely due to the decreased competitiveness of the 30 bp and 40 bp DNA compared to the 50 bp DNA (Figure 4f). This is only observed in the context of yCAF-1 but not in the isolated KERs (Figure 4g) and suggests that the longer hKER can alter the DNA-length preference of yCAF-1. Surprisingly, substitution of the KER for the hKER in yeast had a similar effect as the deletion of the KER, with similar sensitivity to CPT and Zeocin, as well as impaired chromatin silencing when in combination with mWHD (Figure 6d,e and Figure 6-figure supplement 1d). These results indicate that the hKER cannot substitute the yeast KER *in vivo*. Collectively, these results confirm the expected conservation of the overall SAH and DNA-binding characteristics of the KER from different species. Furthermore, and in agreement with our results

in Figure 5, the length of the KER alters the DNA length selectivity and plays a critical role in CAF-1 biological functions.

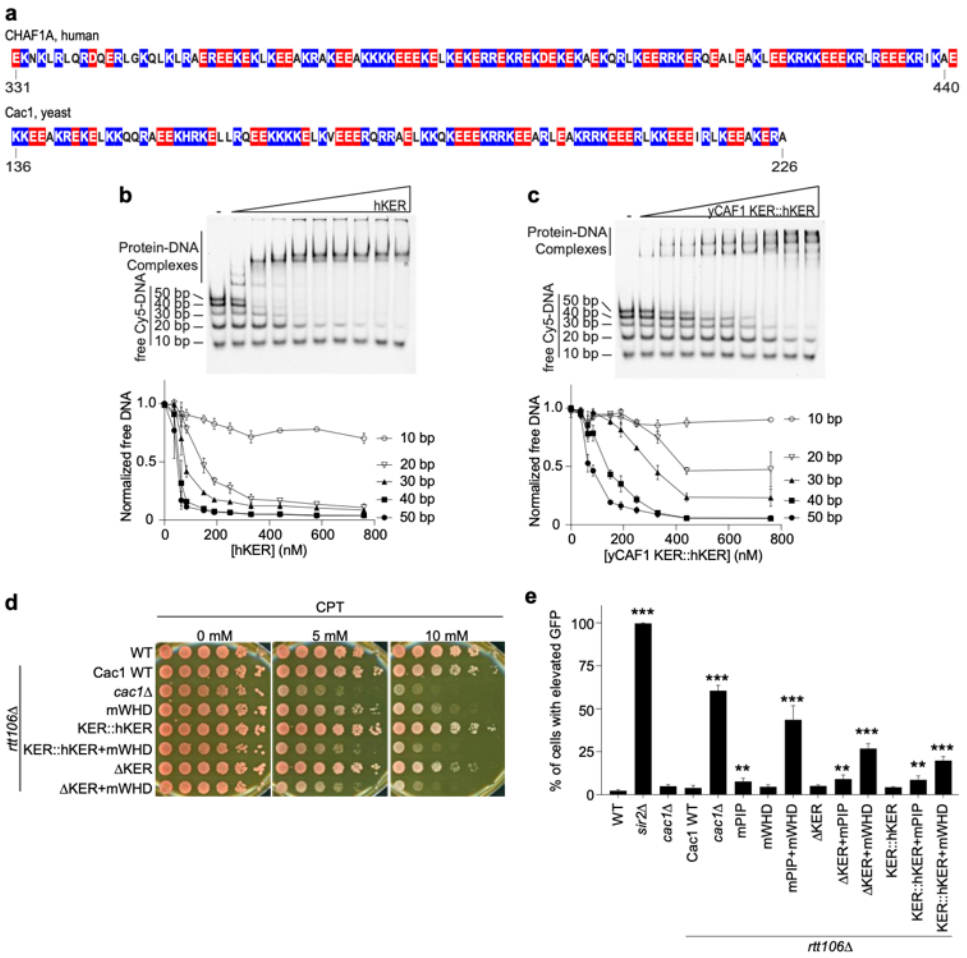

Figure 6. CAF-1 DNA-length selectivity by the KER is species specific and its function is not conserved *in vivo*. a, Sequence of the KER region from human (CHAF1A, top) and yeast (Cac1, bottom) homologues with positively charged residues Arg and Lys colored in blue, and negatively charged residue Glu and Asp colored in red. **b,c,** Images of representative EMSAs of human KER (hKER) and yCAF-1 KER::hKER, were each Cy5-labeled DNA fragment is at 1 nM concentration and the range of protein concentration was 37–760 nM for both constructs. The graphs below show the quantitation of free (unbound) DNA signal for each Cy5-labeled DNA as a function of protein concentration. The data are plotted as the mean and standard deviation (error bars) from at least three measurements. **d,** Yeast spot assay with 5-fold serial dilutions of cultures of the indicated strains; grown in the presence of CPT at the specified concentrations. **e,** Bar graph indicating the percentage of cells exhibiting elevated GFP levels from yeast cultures of the indicated strains sorted by flow cytometry. Error bars indicate the standard deviation of the calculated values from three measurements. Statistical significance was calculated by Student's *t*-test where * = p<0.05, ** = p<0.01, and *** = p<0.001 relative to Cac1 WT cells. See also Figure 6 - Source data 1.

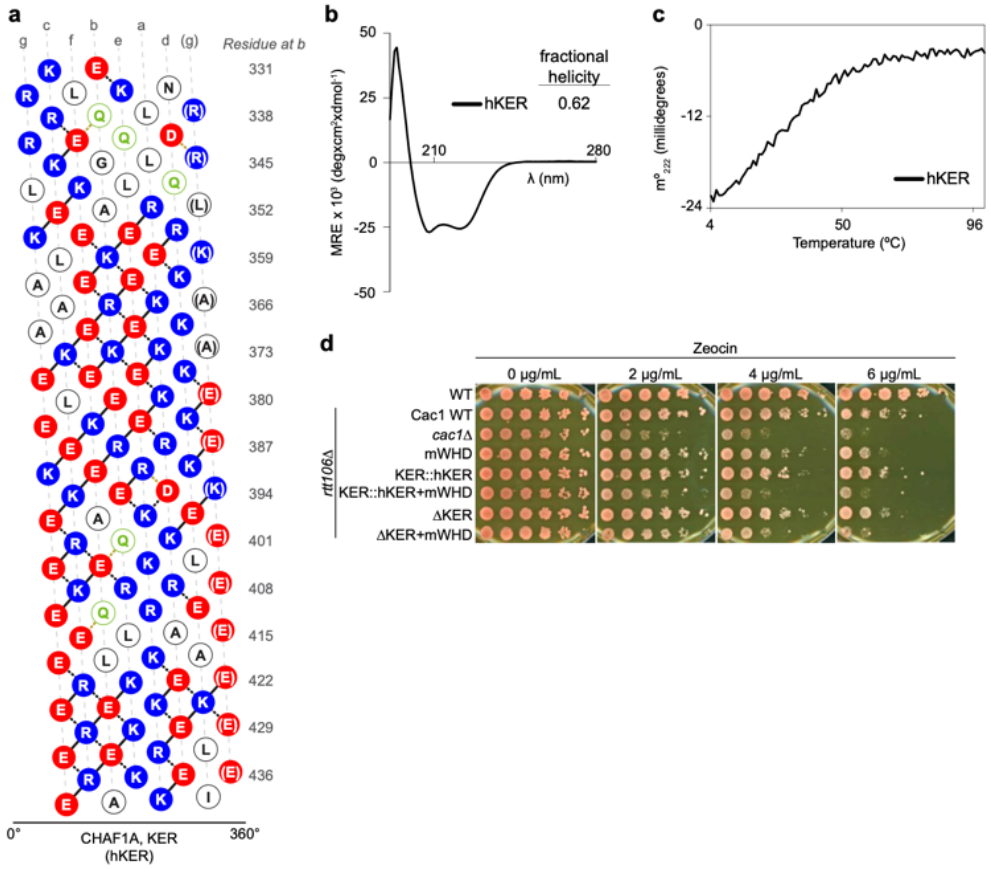

Figure 6-figure supplement 1. Analysis of the substitution of the yKER with the hKER. a, Helical net diagram of the predicted SAH of the hKER (CHAF1A residues 331-441). In this representation, the SAH structure has been split along a helical track and unwound so it can be displayed in 2D, with coloration as in Extended Data Fig.4c. Lines connecting colored residues represent predicted ion pair interactions based on strength: solid lines, strong; black dashed lines, medium; yellow dashed lines, weak. **b,** Circular dichroism spectra of the hKER. **c,** Thermal denaturation monitored by circular dichroism at 222 nm (m^{o}_{222}) of the hKER. **d,** Yeast spot assay with 5-fold serial dilutions of cultures of the indicated strains; grown in the presence of Zeocin at the specified concentrations. See also Figure 6 - figure supplement 1 - Source data 1.

Discussion

The results presented here reveal the structure, activities and function of the KER domain in CAF-1. The KER is a long single alpha helix motif, with a distinct and unique pattern of basic residues. It binds DNA in a non-sequence-specific manner with a binding affinity in the nM range, establishing it as a first-in-class DNA binding domain, namely the 'SAH DBD'. Moreover, we found that in the context of yCAF-1, the KER is largely responsible for observed DNA length-preference of CAF-1 for tetrasome-length DNA (Sauer et al., 2017) and CAF-1 function *in vivo*.

The KER SAH is a novel DNA binding motif.

A defining feature of the SAH motif is the sequence pattern, which produces stabilizing electrostatic-interaction networks along the alpha helix. The KER SAH is the longest SAH described to date (Cac1 aa136-226; 90 aa) with the same general pattern of alternating basic and acidic amino acid residues as classic SAHs (Figure 2) (Sivaramakrishnan et al., 2008; Batchelor et al., 2019; Dudola et al., 2017; Gáspári et al., 2012). However, the KER also has a stripe of basic residues along most of the helix, so far only noticeable in the KER SAH of CAF-1. Also unlike the canonical SAH motif, such as in Myosin 7a, the KER SAH binds to DNA. The appearance of multiple KER-DNA complexes in EMSA supports the role of the KER as a non-sequence-specific DNA binding domain (Churchill et al., 1999; Churchill et al., 1995), consistent with the role of CAF-1 in depositing H3/H4 dimers throughout the genome. The KER of CAF-1 is the first SAH DNA binding domain (SAH-DBD) of its type within the larger group IV of "other alpha-helix DNA binding domains" (Luscombe et al., 2000).Thus, the discovery that the KER is a DNA binding SAH expands the repertoire of DNA binding domains.

The molecular mechanism of KER-DNA recognition requires both key positively charged residues and alpha helical conformation in the Cac1 middle-A section (Figure 3). Although CAF-1 prefers to bind to tetrasome-length DNA (Luger et al., 1997; Donham, Scorgie, and Churchill, 2011), the KER SAH is capable of binding to DNA as short as 20 bp, which is typical of many

DBDs. Many alpha helical DNA binding motifs, including leucine zippers and helix-loop-helix motifs, bind across the DNA within the major groove (Luscombe et al., 2000; Wolberger, 2021; Churchill and Travers, 1991). In contrast, long helices that lie parallel to the DNA exist in chromatin remodelers, such as the HSA and post-HSA domains in the actin related proteins (Arp4 and Arp8) of INO80 (Knoll et al., 2018; Baker et al., 2021). However, these helices simultaneously interact extensively with other polypeptides in addition to the DNA (Knoll et al., 2018; Baker et al., 2021). Whether the KER binds along the length of the DNA or engages only short stretches of the DNA in a similar manner to the other helical motifs is not clear. Our results are consistent with aspects of both models, as the middle region of the KER confers the ability to bind to DNA, and the positively charged amino acids along one face of the SAH DBD would be suitable for recognition along DNA.

Function of the KER SAH-DBD in CAF-1 and implications for nucleosome assembly.

The KER confers the preference of CAF-1 for tetrasome length DNA (Figure 1,4), in spite of the SAH-DBD recognition of shorter DNA lengths (Figure 4). Surprisingly, nearly all perturbations to the KER that we tested in yeast had reduced resistance to DNA damage and loss of gene silencing in combination with the mWHD (Figure 1,5,6 and Table 1), even a deletion of 2 residues, which rotated the helix approximately 200° relative to the DNA or other regions of CAF-1. Although doubling or extending the length of the yKER in yCAF-1 did not change the selectivity for 40 bp DNA, the 2xKER strain overall survived CPT and Zeocin induced DNA damage and maintained gene silencing in the absence of a functional WHD. This suggests that the second KER SAH functionally substitutes for the WHD *in vivo*. We also increased the DNA length preference of yCAF-1 to 50 bp by either derepressing the DNA binding function of the WHD, via the ED:GSL mutation or substituting the yKER with the hKER (Figure 4,6). Both of these mutations provide additional potential DNA binding interactions, but the hKER substitution also had a similar loss of function to the deletion of the KER *in vivo*. Thus, the context of the KER, including molecular

interactions, presence of a viable WHD and structural requirements imposed by the architecture of the CAF-1 complex, is critical for DNA length sensing and CAF-1 function *in vivo*.

How might a DNA length-sensing function of the KER in CAF-1 be relevant during DNA synthesis? One possibility is that extrusion of DNA through PCNA exposes CAF-1 to increasing lengths of naked DNA. The ability of CAF-1 to preferentially bind to a tetrasome length of DNA (Figure 7a) could ensure sufficient DNA is available so that as histone binding releases the WHD, there will be sufficient space along the DNA for the subsequent assembly of tetrasomes, while simultaneously protecting newly replicated DNA from spurious binding of other factors (Ramachandran and Henikoff, 2016). Loss of the KER can be compensated by the WHD (Figure 1,7b), but deletion of both the KER and WHD renders yeast with a reduced ability to survive DNA damage or maintain gene silencing (Figure 7c). Moreover, the yKER is shorter than the KER in humans and many other eukaryotes, and correspondingly preferentially recognizes shorter DNA (Figure 6) than the hKER in the context of yCAF-1, which raises the possibility that the KER serves a spacer function to ensure that tetramers are assembled at specific spacings (Figure 7d). Classic SAHs (Dudola et al., 2017; Gáspári et al., 2012) predominantly use the long rigid helix to bridge two functional domains either as a linker, spacer or flexible spring (Wolny et al., 2014; Wolny et al., 2017; Kwon, Kim, and Lee, 2020; Bandera et al., 2021). Therefore, we propose that the KER SAH acts as a DNA binding physical spacer element and bridge that links with structural precision multiple functional domains within CAF-1 to configure the architecture of CAF-1 for efficient tetrasome assembly after DNA synthesis.

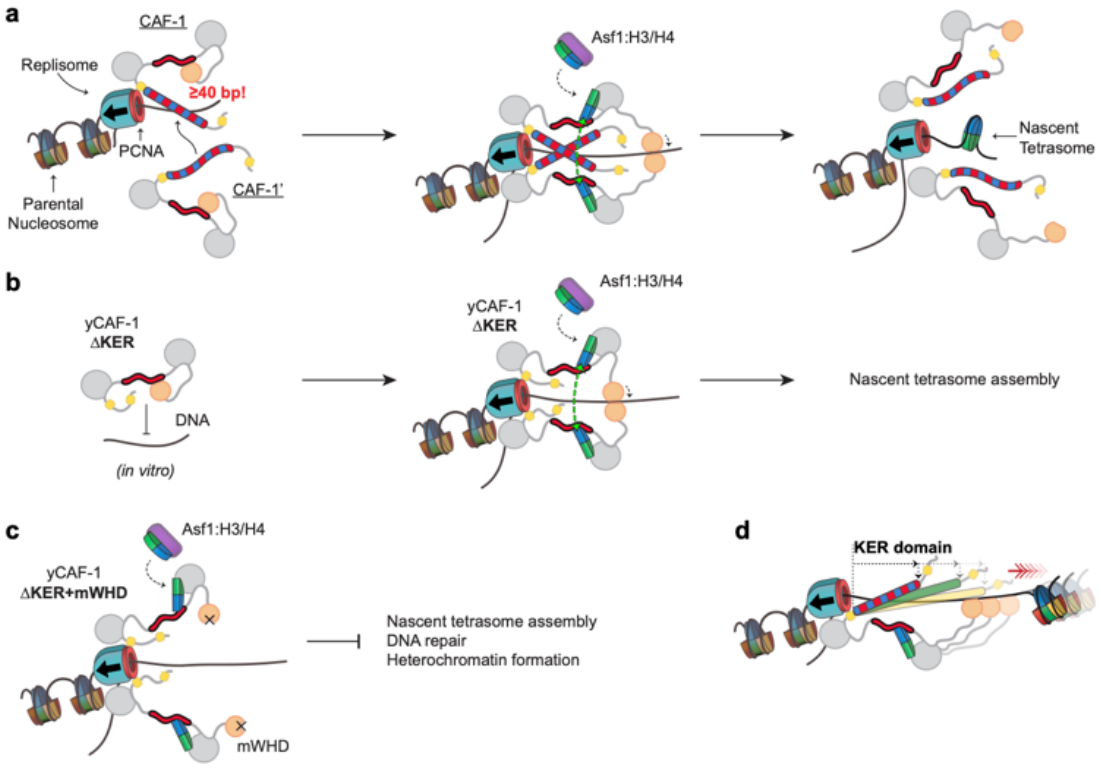

Figure 7. Proposed molecular mechanism model of KER-mediated nascent tetrasome assembly by CAF-1. a, The KER safeguards DNA for tetrasome assembly. Because the KER has strong binding affinity towards DNA and is readily competent for binding, recruitment of CAF-1 to DNA through the KER can be an initial transient state prior to assembly of tetrasomes during DNA replication (left panel). Furthermore, the KER's DNA-length selectivity function equips CAF-1 to bind to free DNA regions that are tetrasome-length (≥ 40 bp). While CAF-1 is bound to DNA through the KER, CAF-1 can receive newly synthesized H3/H4 dimers from the histone chaperone Anti-silencing Function 1 (Asf1) which in turn facilitates DNA binding of the WHD (middle panel). Both, the KER and WHD, bind cooperatively to DNA which facilitate the recruitment of two copies of the CAF-1-H3/H4 complex to the same DNA vicinity (middle panel). A transient DNA-(CAF-1-H3/H4)$_2$ complex provides the conditions to favor the formation of the H3/H4 tetramer (middle panel, green arrows) following its the deposition on DNA and presumably ejecting CAF-1 from the DNA (right panel). **b,c,** Deletion of the KER from yCAF-1 (yCAF-1 ΔKER) impairs binding to DNA *in vitro,* presumably because the WHD binds more weakly to DNA and is in an autoinhibited state. But *in vivo* yCAF-1 ΔKER is still competent for tetrasome assembly with minimal sensitivity to DNA damage and defects on heterochromatin formation. **d,** In contrast, deletion of the KER (ΔKER) in combination with inhibition of the DNA binding function of the WHD (mWHD) dramatically impairs DNA repair and heterochromatin formation functions of yCAF-1 *in vivo*. Because in ΔKER+mWHD cells yCAF-1 has no detectable functional DNA binding domain, tetrasome formation cannot occur efficiently. **d,** The length of the KER domain in CAF-1 varies across species and it can alter the DNA-length recognized by CAF-1 *in vitro*, which could alter tetrasome assembly during DNA replication.

Materials and Methods

Expression and purification of Cac1 subunits and CAF-1 proteins from insect cells.

For expression in insect cells, baculoviruses harboring yCAF-1 subunits and mutants were made using the Gateway technology subcloning system (Thermo Fisher Scientific). The pDONR/Zeo plasmid containing the sequence encoding Cac1 subunit (Cac1, pDONR/Zeo; Supplementary Table 1) was used for mutagenesis experiments. Briefly, the Cac1, pDONR/Zeo plasmid was linearized via Polymerase Chain Reaction (PCR) with the Q5 DNA polymerase (NEB) and a pair of primers for each Cac1 mutant that anneal to the sequences flanking the section to be modified (Supplementary Table 2). The primers also had complementary sequences with overhangs: to each other for deletion of Cac1 regions, or to a double-stranded DNA fragment either synthetically manufactured (Integrated DNA Technologies) or PCR-amplified from cDNA for the exogenous incorporation of other genes or duplication of Cac1 sequences (Supplementary Table 2). Circularization of the modified Cac1, pDONR/Zeo (Supplementary Table 1) plasmid with the desired mutation was done via In-Fusion technology (Takara). Each pDONR/Zeo Cac1 mutant plasmid was verified by Sanger sequencing. Cac1 mutants from the pDONR/Zeo plasmids were then sub-cloned into the pDEST8 vector via Gateway technology (Thermo Fisher Scientific) followed by Sanger sequencing verification (Supplementary Table 1). Finally, to generate Baculovirus stocks of each Cac1 mutant, we used the Bac-to-Bac system (Thermo Fisher Scientific), where the generated pDEST8 plasmids were transformed into DH10Bac E. coli cells (Thermo Fisher Scientific) to generated bacmids competent for baculovirus production in Sf9 cells (Thermo Fisher Scientific) via transfection. Media containing secreted baculovirus from cultured Sf9 cells was stored at 4 ºC and used for subsequent protein production.

Full-length yCAF-1 and complex mutants were expressed for 72 hours in High Five cells (Thermo Fisher Scientific) infected with a baculovirus stock of Cac1 with a C-terminal Strep II epitope, Cac2 with a C-terminal His_6 or Strep II epitope, and Cac3 with a C-terminal 3xFLAG epitope. Purification of the CAF-1 complexes was carried out as before (Liu et al., 2012) where

cell pellets were homogenized in 20 mM HEPES pH 7.4, 350 mM NaCl, 1 mM DTT, 10 µg/mL DNase I, 1 mM Na_3VO_4, 10 mM NaF, 1mM PMSF, and a cocktail of protease inhibitors (Tablet EDTA-free, Sigma). Homogenate was clarified by centrifugation at 10 000 g for 45 min. at 4 ºC, followed by affinity chromatography with a StrepTrap HP column (Cytiva) and washed extensively with 20 mM HEPES pH 7.4, 350 mM NaCl, and 0.5 mM TCEP. Protein was eluted with the wash buffer containing 2.5 mM d-Desthiobiotin (MilliporeSigma). Purified yCAF-1 complexes (Figure 1-figure supplement 1a) were concentrated with 100 000 MWCO centrifugal concentrators (Sartorius), aliquoted in small volumes, flash frozen in liquid nitrogen, and stored at -80 ºC.

Expression and purification of CAF-1 domains and Myosin 7a SAH from *E. coli*.

Plasmids for bacterial expression were generated using the Gateway technology subcloning system (Thermo Fisher Scientific). The initial double-stranded DNA insert containing the cDNA that encodes for the protein of interest was obtained either synthetically manufactured (Integrated DNA Technologies) or by PCR amplification from cDNA of a plasmid containing the full-length protein (Supplementary Table 2). To obtain the double-stranded DNA insert for human KER, E. coli codon optimized CHAF1A cDNA was first cloned into a pGEX-6P-1 vector via In Fusion (Takara) (Supplementary Table 3). For Gateway cloning, the double-stranded DNA inserts were subcloned into the pDONR/Zeo and pDEST566 vectors followed by Sanger sequencing verification of each plasmid (Supplementary Table 1).

Yeast Cac1 KER constructs (full-length and truncations), human CHAF1A KER, and Myosin 7 SAH cloned into the pDEST566 vector produced an N-terminal His_6-MBP-tagged polypeptide with a PreScission protease site downstream of the MBP. Proteins used in CD or EMSA experiments contained an exogenous Tyrosine amino acid as the very last C-terminal residue to facilitate the determination of protein concentration via UV absorption after removal of the His_6-MBP tag. Expression of the His_6-MBP-tagged proteins were carried out in Rosetta 2 (DE3) pLysS cells cultured in Luria Broth media at 37 ºC. Bacterial cultures were induced for

646 expression with 0.5 mM IPTG when culture reached a 600 nm optical density of 0.8 and let
647 incubate for another 3 to 4 hours at 37 ºC. Subsequently, cell pellets were harvested and
648 resuspended in 25 mM Tris pH 7.5, 50 mM NaCl, 10 µg/mL DNaseI, 1 mM PMSF, and a cocktail
649 of protease inhibitors (Tablet EDTA-free, Roche). The lysate was sonicated and then clarified by
650 centrifugation at 10,000 g for 45 min at 4 ºC. The resulting supernatant was then bound to an
651 agarose Ni-NTA resin (Qiagen) and incubated for at least 2 hours at 4 ºC followed by extensive
652 washes with 25 mM Tris pH 7.5, 1 M NaCl and 1 mM PMSF. Protein was eluted from the Ni-NTA
653 resin with 25 mM Tris pH 7.5, 20 mM NaCl, 500 mM Imidazole and 1 mM PMSF, and further
654 purified by ion exchange chromatography using an SP FF or Source S15 column (Cytiva) with a
655 30-column volumes salt gradient from 20 mM to 1 M NaCl for elution. Purified His_6-MBP-tagged
656 proteins were then concentrated with a 30,000 MWCO centrifugal concentrator (Sartorius) and
657 buffer exchanged into 20 mM HEPES pH 7.5 and 50 mM NaCl for crystallization, or in 50 mM Tris
658 pH 7.5, 150 mM NaCl, 1 mM EDTA, 1 mM DTT and 0.01 % Triton X-100 for enzymatic removal
659 of the His_6-MBP tag with PreScission protease. PreScission protease was added to the His_6-MBP-
660 tagged proteins and incubated overnight at 4 ºC. Cleaved proteins were further purified by ion
661 exchanged as described above, followed by concentration with a 3,000 MWCO and buffer
662 exchange into 20 mM HEPES pH 7.5, 150 mM NaCl, and 0.2 mM TCEP (Figure 1-figure
663 supplement 1b). Concentrated proteins were aliquoted in small volumes, flash frozen in liquid
664 nitrogen, and stored at -80 ºC.

665 The Cac1 WHD construct was expressed and purified as before (Liu et al., 2016) using
666 the Cac1 WHD, pGEX-6P-1 plasmid (Supplementary Table 1).

667

668 **Preparation of DNA templates.**

669 DNA fragments of varying lengths were designed around the dyad of the 147 bp 601 DNA
670 sequence (Lowary and Widom, 1998; Luger et al., 1997). Synthetic oligonucleotides for

671 production of dsDNA (Integrated DNA Technologies) had only one strand containing a Cy5
672 fluorophore at the 5' end (Supplementary Table 2).
673 Each oligonucleotide was resuspended in 10 mM Tris-HCl and 1 mM EDTA at pH 8.0 (TE
674 buffer) and non-fluorophore labeled oligonucleotides were purified using C18 Sep-Pak cartridges
675 (Waters). Annealing of complementary oligonucleotides was done by heating an equimolar
676 combination of each strand at 95 ºC and then cooling slowly to room temperature in TE Buffer
677 with 5 mM NaCl. Annealed DNA duplexes were purified by ion exchange chromatography using
678 a DEAE column (Tosoh Bioscience) under a gradient of 0 to 1 M NaCl in TE Buffer. Purified DNA
679 was ethanol precipitated and resuspended in TE Buffer.
680 The 10 to 100 bp DNA step ladder was purchased from Promega (Cat. G447A).
681
682 **Electrophoretic mobility shift assays (EMSA).**
683 Increasing concentrations of protein that ranged from 9 nM to 10 μM were incubated with 1
684 or 3 nM of Cy5-labeled DNA in 20 mM HEPES pH 7.4, 150 mM NaCl and 0.5 mM TCEP for 1
685 hour on ice. The Protein-DNA species were separated by electrophoresis in 0.2X TBE 4, 5, 6, or
686 10 % 59:1 acrylamide:bis-acrylamide native gels for 60 min. at 70 V on ice. Fluorescence from
687 the Cy5 fluorophore was detected by imaging the native gels on a c600 (Azure Biosystem) or a
688 Sapphire Biomolecular (Azure Biosystems) imager. To determine dissociation constants between
689 the Protein and DNA substrates, the intensity of each DNA band was determined using the
690 AzureSpot software (Azure Biosystems), followed by background subtraction and calculation of
691 the DNA fraction bound. Finally, Protein concentrations ([Protein]) and DNA fraction bound values
692 were plotted and the binding curves fitted with Equation 1 using the Prism software (GraphPad):
693 Eqn 1.

694 $$\text{Fraction Bound} = \frac{B_{max} \times [\text{Protein}]^h}{{K_D}^h + [\text{Protein}]^h}$$

695 where h corresponds to the Hill coefficient, K_D is the dissociation constant and B_{max} represents

maximum binding. All EMSA experiments were done at least three times and the reported K_D values and Hill coefficients correspond to the average of the multiple measurements. Error bars represent the standard deviation.

EMSA experiments using the commercial 10 bp DNA step ladder substrate contained 500 nM total DNA and gels were stained with SYBR Green I stain (Invitrogen) prior to imaging.

In the Cy5-DNA ladder assay, the signal of the free DNA of a particular fragment from subsequent protein titration was normalized to the signal of the free DNA in the absence of protein (normalized free DNA). To obtain the protein concentrations at which 50% of the DNA was depleted, we first fitted binding curves (Eqn. 1) to the data and selected the protein concentration at which 50% of the DNA on each curve occurred, using the error range of the 95% confidence limit for the fitted curve.

Structure determination and analyses.

The His_6-MBP-yKER (Cac1 residues 136–225) protein was expressed and purified as described above and protein was concentrated to 25 mg/mL in 20 mM HEPES pH 7.5 and incubated with 200 mM NDSB-256. Protein crystals grew in 0.1 M Phosphate/citrate pH 4.2 and 30 % PEG 300 using the hanging drop vapor diffusion method at 15 ºC. Data were collected using a Rigaku Micromax 007 high flux microfocus X-ray generator equipped with a VariMax high flux optic, an AFC11 4-axis goniometer, a Pilatus 200K 2D area detector, and an Oxford cryo-system. Data were initially processed using the HKL-3000R software (HKL Research Inc.) and phased by molecular replacement using the structure of MBP (PDB ID: 1PEB) as the search model (Telmer and Shilton, 2003). The structure was solved at a resolution of 2.81 Å. The model was built using COOT (Emsley and Cowtan, 2004) and refinement was conducted using PHENIX (Afonine et al., 2012), to achieve acceptable geometry and stereochemistry. Group TLS refinement was used in the refinement as there were large regions of chain, with much higher than average B-factors. Several sections of chain D are poorly defined due to this disorder. The quality of the structure

722 (PDB ID: 8DEI) was analyzed (Supplementary Table 4) and the root mean squared deviation
723 (R.M.S.D.) values were calculated using PyMol and COOT. Figures were made using PyMol and
724 Photoshop (Adobe).
725
726 **Circular Dichroism (CD) spectroscopy.**
727 Proteins were prepared for CD at a concentration of 0.1 mg/mL in 10 mM Na-Phosphate
728 Buffer at pH 7.4 and 50 mM NaCl. KER samples containing DNA were mixed at 1:1 molar
729 concentration of protein and 40 bp 601 DNA. All samples were analyzed in a cuvette with a path
730 length of 1 mm on a Jasco J-815 CD Spectrophotometer equipped with a Lauda Brinkman ecoline
731 RE 106 temperature controller. CD was measured in millidegrees from 185 to 350 nm
732 wavelengths with a bandpass of 1 nm and a step size of 1.0 nm. Six scans of each sample were
733 averaged per experiment with at least three independent replicates. Equation 2 was used to
734 calculate Mean Residue Ellipticity (MRE) (Woody, 1996):
735 Eqn. 2

736 $$\mathrm{MRE} = \frac{\mathrm{m}^0 \times \frac{\mathrm{MW}}{\mathrm{n}-1}}{10 \times \mathrm{L} \times \mathrm{C}}$$

737 Where m^0 is the observed ellipticity in millidegrees, MW is the molecular weight of the protein in
738 g/mol, n is the number of residues of the protein, L is the path length of cell, and C is the
739 concentration of the protein in g/L.
740 To calculate the fractional helicity of a protein sample, we used the 222 nm wavelength
741 method (Wei, Thyparambil, and Latour, 2014) (Eqn. 3):
742 Eqn. 3

743 $$\text{fractional helicity} = \frac{\theta_{222}^{\exp} - \theta_{222}^{\mathrm{u}}}{\theta_{222}^{\mathrm{h}} - \theta_{222}^{\mathrm{u}}}$$

744 where $\theta_{222}^{\exp}$ is the experimentally observed MRE at 222 nm of the protein sample, and $\theta_{222}^{\mathrm{u}}$ and
745 $\theta_{222}^{\mathrm{h}}$ are the MRE at 222 nm of a protein with 0 % and 100 % helical content which are estimated

to be -3 000 and -39 000 degxcmxdmol^{-1}, respectively.

Chemical crosslinking.

DSS crosslinker (Thermo Pierce) was prepared at 2 mM by dissolution in DMSO. 10 µM yKER (Cac1 residues 136 – 225 with additional C'-terminal Tyrosine) was allowed to incubate with 200 µM DSS or DMSO for 30 min at room temperature in 10 mM Phosphate Buffer at pH 7.5, 150 mM NaCl, and 0.5 mM TCEP. The cross-linking reaction was quenched by addition of 50 mM Tris pH 7.4 and incubated for an additional 15 min. The reactions were resolved in a 4 –15 % Tris-HCl SDS-PAGE (BioRad) and stained with Coomassie Blue.

Yeast strains and primers.

The yeast strains used in this study and their genotypes are fully described in Supplementary Table 3. Strains used in DNA damage sensitivity assays and western blotting were isogenic to W303-1a (Thomas and Rothstein, 1989), while strains used to assay silencing at the *HMR* locus were isogenic to BY4741(Baker Brachmann et al., 1998). Mutations in the *CAC1* gene were made using CRISPR-Cas9 (Ryan, Poddar, and Cate, 2016) to mutate the endogenous *CAC1* (RLF2) locus. Sequences of gRNA and HDR template DNA used to generate each mutant are listed in Supplementary Table 2. Where indicated, strains were deleted for *RTT106* or *CAC1* using pFA6a-HIS3MX6 (Longtine et al., 1998) and pFA6a-KANMX6 (Bähler et al., 1998) respectively.

DNA damage sensitivity assay.

Cells were grown in YPD media until reaching mid-log phase (OD 0.8-1.0). They were collected by centrifugation, resuspended in sterile water, and five-fold serially diluted before spotting onto YPD agar plates containing the indicated concentrations of the DNA-damaging

771 drugs Zeocin (Invitrogen R25001) or CPT (Cayman Chemical 11694). Plates were grown for 3
772 days at 30°C before imaging.
773
774 **Measurement of loss of silencing at the *HMR* locus.**
775 To observe loss of silencing at the *HMR* locus, cells isogenic to BY4741 were transformed
776 with the plasmid pHMR::P_{URA3}-GFP/URA3 after EcoRI/XhoI digestion (Laney and Hochstrasser,
777 2003). In WT cells, this GFP reporter is silenced, while mutants with loss of silencing express
778 GFP at varying levels that was detected by flow cytometry (Huang et al., 2005). 0.5 mL of mid-
779 log phase (OD 0.8-1.0) cells growing in synthetic complete (SC) media containing 2% dextrose
780 were collected by centrifugation, washed twice with ice-cold PBS, and resuspended in 1 mL of
781 PBS before analysis on a flow cytometer (BD Biosciences BD® LSR II). Cells deleted for *SIR2*
782 (*sir2*Δ) have a severe silencing defect and were used as a positive control. As indicated in Figure
783 1-figure supplement 2f, a gate containing <1 % of WT cells and >97 % of *sir2*Δ cells was drawn
784 and used to identify the percent of cells with loss of silencing. As previously observed, the
785 percentage of WT cells with loss of silencing varied from ~0.3-2.5 % across experiments. Data is
786 presented as the average ± standard deviation of at least three experiments performed on
787 independent yeast colonies.
788
789 **Western blot for Cac1-FLAG.**
790 1 OD of cells with an endogenous C-terminal FLAG tag on *CAC1* were grown in YPD to
791 mid-log phase, collected, flash-frozen in liquid nitrogen, resuspended in 100 μL of modified
792 Laemmli buffer (Horvath and Riezman, 1994), and boiled for 5 minutes. Proteins were separated
793 on a 10% SDS-PAGE gel and Western blotting was performed using anti-FLAG M2 (Sigma
794 F3165) and anti-GAPDH (Sigma A9521).
795

Data Availability

Diffraction data have been deposited in the PDB under the accession code 8DEI. All plasmids are available by request.

Acknowledgements

We appreciate the contributions of Dr. Ying-Chih Chi for preparing the initial CHAF1A expression plasmid and Dr. Mark Hochstrasser for providing the pHMR::PURA3-GFP/URA3 plasmid to us. We thank the Biophysical core facility at CU-Anschutz for experimental advice and assistance, as well as the Structural Biology Shared Resources of the University of Colorado Cancer Center supported by NIH P30 CA046934. This work was supported by NIH R01 GM135604 to M.E.A.C., R01 CA95641 to J.K.T. and NIH Shared instrumentation grant S10 OD012033. R.R.A. was supported by a Medical Scientist Training Program grant from the National Institute of General Medical Sciences of the National Institutes of Health under award number: T32GM007739 to the Weill Cornell/Rockefeller/Sloan Kettering Tri-Institutional MD-PhD Pro-gram, and a diversity supplement on grant RO1 GM64475 to J.K.T.

Competing Interests

JKT, eLife Senior Editor

References

Afonine, Pavel V., Ralf W. Grosse-Kunstleve, Nathaniel Echols, Jeffrey J. Headd, Nigel W. Moriarty, Marat Mustyakimov, Thomas C. Terwilliger, Alexandre Urzhumtsev, Peter H. Zwart, and Paul D. Adams. 2012. 'Towards automated crystallographic structure refinement with phenix.refine', *Acta Crystallographica Section D: Biological Crystallography*, 68: 352-67.

Bähler, Jürg, Jian-Qiu Wu, Mark S. Longtine, Nirav G. Shah, Amos McKenzie Iii, Alexander B. Steever, Achim Wach, Peter Philippsen, and John R. Pringle. 1998. 'Heterologous modules for efficient and versatile PCR-based gene targeting in Schizosaccharomyces pombe', *Yeast*, 14: 943-51.

Baker Brachmann, Carrie, Adrian Davies, Gregory J. Cost, Emerita Caputo, Joachim Li, Philip Hieter, and Jef D. Boeke. 1998. 'Designer deletion strains derived from Saccharomyces cerevisiae S288C: A useful set of strains and plasmids for PCR-mediated gene disruption and other applications', *Yeast*, 14: 115-32.

Baker, Richard W., Janice M. Reimer, Peter J. Carman, Bengi Turegun, Tsutomu Arakawa, Roberto Dominguez, and Andres E. Leschziner. 2021. 'Structural insights into assembly and function of the RSC chromatin remodeling complex', *Nature Structural & Molecular Biology*, 28: 71-80.

Bandera, Adrian M, Joseph Bartho, Katja Lammens, David Jan Drexler, Jasmin Kleinschwärzer, Karl-Peter Hopfner, and Gregor Witte. 2021. 'BusR senses bipartite DNA binding motifs by a unique molecular ruler architecture', *Nucleic Acids Research*, 49: 10166-77.

836 Barnes, C. Ashley, Yang Shen, Jinfa Ying, Yasuharu Takagi, Dennis A. Torchia, James R.
837 Sellers, and Ad Bax. 2019. 'Remarkable Rigidity of the Single α-Helical Domain of
838 Myosin-VI As Revealed by NMR Spectroscopy', *Journal of the American Chemical*
839 *Society*, 141: 9004-17.

840 Batchelor, Matthew, Marcin Wolny, Emily G. Baker, Emanuele Paci, Arnout P. Kalverda, and
841 Michelle Peckham. 2019. 'Dynamic ion pair behavior stabilizes single α-helices in
842 proteins', *Journal of Biological Chemistry*, 294: 3219-34.

843 Chankova, S. G., E. Dimova, M. Dimitrova, and P. E. Bryant. 2007. 'Induction of DNA double-
844 strand breaks by zeocin in Chlamydomonas reinhardtii and the role of increased DNA
845 double-strand breaks rejoining in the formation of an adaptive response', *Radiation and*
846 *Environmental Biophysics*, 46: 409-16.

847 Cheloufi, Sihem, Ulrich Elling, Barbara Hopfgartner, Youngsook L. Jung, Jernej Murn, Maria
848 Ninova, Maria Hubmann, Aimee I. Badeaux, Cheen Euong Ang, Danielle Tenen, Daniel
849 J. Wesche, Nadezhda Abazova, Max Hogue, Nilgun Tasdemir, Justin Brumbaugh,
850 Philipp Rathert, Julian Jude, Francesco Ferrari, Andres Blanco, Michaela Fellner, Daniel
851 Wenzel, Marietta Zinner, Simon E. Vidal, Oliver Bell, Matthias Stadtfeld, Howard Y.
852 Chang, Genevieve Almouzni, Scott W. Lowe, John Rinn, Marius Wernig, Alexei Aravin,
853 Yang Shi, Peter J. Park, Josef M. Penninger, Johannes Zuber, and Konrad
854 Hochedlinger. 2015. 'The histone chaperone CAF-1 safeguards somatic cell identity',
855 *Nature*, 528: 218-24.

856 Cheloufi, Sihem, and Konrad Hochedlinger. 2017. 'Emerging roles of the histone chaperone
857 CAF-1 in cellular plasticity', *Current Opinion in Genetics and Development*, 46: 83-94.

Churchill, M. E., D. N. Jones, T. Glaser, H. Hefner, M. A. Searles, and A. A. Travers. 1995. 'HMG-D is an architecture-specific protein that preferentially binds to DNA containing the dinucleotide TG', *The EMBO Journal*, 14: 1264-75.

Churchill, Mair E. A., Anita Changela, Linda K. Dow, and Adam J. Krieg. 1999. 'Interactions of high mobility group box proteins with DNA and chromatin.' in, *Methods in Enzymology* (Academic Press).

Churchill, Man E. A., and Andrew A. Travers. 1991. 'Protein motifs that recognize structural features of DNA', *Trends in Biochemical Sciences*, 16: 92-97.

Donham, Douglas C., Jean K. Scorgie, and Mair E. A. Churchill. 2011. 'The activity of the histone chaperone yeast Asf1 in the assembly and disassembly of histone H3/H4–DNA complexes', *Nucleic Acids Research*, 39: 5449-58.

Dudola, Dániel, Gábor Tóth, László Nyitray, and Zoltán Gáspári. 2017. 'Consensus Prediction of Charged Single Alpha-Helices with CSAHserver.' in Yaoqi Zhou, Andrzej Kloczkowski, Eshel Faraggi and Yuedong Yang (eds.), *Prediction of Protein Secondary Structure* (Springer New York: New York, NY).

Emsley, P., and K. Cowtan. 2004. 'Coot: model-building tools for molecular graphics', *Acta Crystallographica. Section D: Biological Crystallography*, 60: 2126-32.

Eng, W. K., L. Faucette, R. K. Johnson, and R. Sternglanz. 1988. 'Evidence that DNA topoisomerase I is necessary for the cytotoxic effects of camptothecin', *Molecular Pharmacology*, 34: 755.

878 Escobar, Thelma M., Alejandra Loyola, and Danny Reinberg. 2021. 'Parental nucleosome
879 segregation and the inheritance of cellular identity', *Nature Reviews Genetics*, 22: 379-
880 92.

881 Gaillard, P. H., E. M. Martini, P. D. Kaufman, B. Stillman, E. Moustacchi, and G. Almouzni.
882 1996. 'Chromatin assembly coupled to DNA repair: a new role for chromatin assembly
883 factor I', *Cell*, 86: 887-96.

884 Gangelhoff, Todd A., Purnima S. Mungalachetty, Jay C. Nix, and Mair E. A. Churchill. 2009.
885 'Structural analysis and DNA binding of the HMG domains of the human mitochondrial
886 transcription factor A', *Nucleic Acids Research*, 37: 3153-64.

887 Gáspári, Zoltán, Dániel Süveges, András Perczel, László Nyitray, and Gábor Tóth. 2012.
888 'Charged single alpha-helices in proteomes revealed by a consensus prediction
889 approach', *Biochimica et Biophysica Acta (BBA) - Proteins and Proteomics*, 1824: 637-
890 46.

891 Hope, I. A., and K. Struhl. 1987. 'GCN4, a eukaryotic transcriptional activator protein, binds as a
892 dimer to target DNA', *The EMBO Journal*, 6: 2781-84.

893 Horvath, Anton, and Howard Riezman. 1994. 'Rapid protein extraction from Saccharomyces
894 cerevisiae', *Yeast*, 10: 1305-10.

895 Huang, Shengbing, Hui Zhou, David Katzmann, Mark Hochstrasser, Elena Atanasova, and
896 Zhiguo Zhang. 2005. 'Rtt106p is a histone chaperone involved in heterochromatin-

mediated silencing', *Proceedings of the National Academy of Sciences of the United States of America*, 102: 13410-15.

Kaufman, P. D., R. Kobayashi, N. Kessler, and B. Stillman. 1995. 'The p150 and p60 subunits of chromatin assembly factor I: a molecular link between newly synthesized histones and DNA replication', *Cell*, 81: 1105-14.

Klemm, Sandy L., Zohar Shipony, and William J. Greenleaf. 2019. 'Chromatin accessibility and the regulatory epigenome', *Nature Reviews Genetics*, 20: 207-20.

Knoll, Kilian R., Sebastian Eustermann, Vanessa Niebauer, Elisa Oberbeckmann, Gabriele Stoehr, Kevin Schall, Alessandro Tosi, Marianne Schwarz, Andrea Buchfellner, Philipp Korber, and Karl-Peter Hopfner. 2018. 'The nuclear actin-containing Arp8 module is a linker DNA sensor driving INO80 chromatin remodeling', *Nature Structural & Molecular Biology*, 25: 823-32.

Krawitz, Denise C., Tamar Kama, and Paul D. Kaufman. 2002. 'Chromatin assembly factor I mutants defective for PCNA binding require Asf1/Hir proteins for silencing', *Molecular and Cellular Biology*, 22: 614-25.

Kwon, Na-Young, Youngjin Kim, and Jie-Oh Lee. 2020. 'The application of helix fusion methods in structural biology', *Current Opinion in Structural Biology*, 60: 110-16.

Laney, Jeffrey D., and Mark Hochstrasser. 2003. 'Ubiquitin-dependent degradation of the yeast Matα2 repressor enables a switch in developmental state', *Genes and Development*, 17: 2259-70.

Li, Q., H. Zhou, H. Wurtele, B. Davies, B. Horazdovsky, A. Verreault, and Z. Zhang. 2008a. 'Acetylation of histone H3 lysine 56 regulates replication-coupled nucleosome assembly', *Cell*, 134: 244-55.

Li, Qing, Hui Zhou, Hugo Wurtele, Brian Davies, Bruce Horazdovsky, Alain Verreault, and Zhiguo Zhang. 2008b. 'Acetylation of histone H3 lysine 56 regulates replication-coupled nucleosome assembly', *Cell*, 134: 244-55.

Liu, Wallace H., Sarah C. Roemer, Alex M. Port, and Mair E. A. Churchill. 2012. 'CAF-1-induced oligomerization of histones H3/H4 and mutually exclusive interactions with Asf1 guide H3/H4 transitions among histone chaperones and DNA', *Nucleic Acids Research*, 40: 11229-39.

Liu, Wallace H., Sarah C. Roemer, Yeyun Zhou, Zih-Jie Shen, Briana K. Dennehey, Jeremy L. Balsbaugh, Jennifer C. Liddle, Travis Nemkov, Natalie G. Ahn, Kirk C. Hansen, Jessica K. Tyler, and Mair E. A. Churchill. 2016. 'The Cac1 subunit of histone chaperone CAF-1 organizes CAF-1-H3/H4 architecture and tetramerizes histones', *eLife*, 5.

Longtine, Mark S., Amos McKenzie Iii, Douglas J. Demarini, Nirav G. Shah, Achim Wach, Arndt Brachat, Peter Philippsen, and John R. Pringle. 1998. 'Additional modules for versatile and economical PCR-based gene deletion and modification in Saccharomyces cerevisiae', *Yeast*, 14: 953-61.

Lowary, P. T., and J. Widom. 1998. 'New DNA sequence rules for high affinity binding to histone octamer and sequence-directed nucleosome positioning', *Journal of Molecular Biology*, 276: 19-42.

938 Luger, Karolin, Armin W. Mäder, Robin K. Richmond, David F. Sargent, and Timothy J.
939 Richmond. 1997. 'Crystal structure of the nucleosome core particle at 2.8 Å resolution',
940 *Nature*, 389: 251-60.

941 Luscombe, Nicholas M., Susan E. Austin, Helen M. Berman, and Janet M. Thornton. 2000. 'An
942 overview of the structures of protein-DNA complexes', *Genome Biology*, 1:
943 reviews001.1.

944 Mattiroli, Francesca, Yajie Gu, Tejas Yadav, Jeremy L. Balsbaugh, Michael R. Harris, Eileen S.
945 Findlay, Yang Liu, Catherine A. Radebaugh, Laurie A. Stargell, Natalie G. Ahn, Iestyn
946 Whitehouse, and Karolin Luger. 2017a. 'DNA-mediated association of two histone-bound
947 CAF-1 complexes drives tetrasome assembly in the wake of DNA replication', *eLife*, 6:
948 e22799-e99.

949 ———. 2017b. 'DNA-mediated association of two histone-bound complexes of yeast Chromatin
950 Assembly Factor-1 (CAF-1) drives tetrasome assembly in the wake of DNA replication',
951 *eLife*, 6.

952 Mello, J. A., H. H. Sillje, D. M. Roche, D. B. Kirschner, E. A. Nigg, and G. Almouzni. 2002.
953 'Human Asf1 and CAF-1 interact and synergize in a repair-coupled nucleosome
954 assembly pathway', *EMBO Rep*, 3: 329-34.

955 Pommier, Yves. 2006. 'Topoisomerase I inhibitors: camptothecins and beyond', *Nature Reviews*
956 *Cancer*, 6: 789-802.

957 Ramachandran, Srinivas, and Steven Henikoff. 2016. 'Transcriptional Regulators Compete with
958 Nucleosomes Post-replication', *Cell*, 165: 580-92.

959 Rine, Jasper, and Ira Herskowitz. 1987. 'Four Genes Responsible for a Position Effect on
960 Expression From HML and HMR in Saccharomyces cerevisiae', *Genetics*, 116: 9-22.

961 Ryan, Owen W., Snigdha Poddar, and Jamie H. D. Cate. 2016. 'CRISPR–Cas9 Genome
962 Engineering in Saccharomyces cerevisiae Cells', *Cold Spring Harbor Protocols*, 2016:
963 pdb.prot086827.

964 Sauer, Paul V., Yajie Gu, Wallace H. Liu, Francesca Mattiroli, Daniel Panne, Karolin Luger, and
965 Mair E. A. Churchill. 2018. 'Mechanistic insights into histone deposition and nucleosome
966 assembly by the chromatin assembly factor-1', *Nucleic Acids Research*.

967 Sauer, Paul Victor, Jennifer Timm, Danni Liu, David Sitbon, Elisabetta Boeri-Erba, Christophe
968 Velours, Norbert Mücke, Jörg Langowski, Françoise Ochsenbein, Geneviève Almouzni,
969 and Daniel Panne. 2017. 'Insights into the molecular architecture and histone H3-H4
970 deposition mechanism of yeast Chromatin assembly factor 1', *eLife*, 6.

971 Shibahara, K., and B. Stillman. 1999. 'Replication-dependent marking of DNA by PCNA
972 facilitates CAF-1-coupled inheritance of chromatin', *Cell*, 96: 575-85.

973 Sivaramakrishnan, Sivaraj, J. Spink Benjamin, Y. L. Sim Adelene, Sebastian Doniach, and A.
974 Spudich James. 2008. 'Dynamic charge interactions create surprising rigidity in the ER/K
975 α-helical protein motif', *Proceedings of the National Academy of Sciences of the United*
976 *States of America*, 105: 13356-61.

977 Smith, Duncan J., and Iestyn Whitehouse. 2012. 'Intrinsic coupling of lagging-strand synthesis
978 to chromatin assembly', *Nature*, 483: 434-38.

979 Smith, S., and B. Stillman. 1989. 'Purification and characterization of CAF-I, a human cell factor
980 required for chromatin assembly during DNA replication in vitro', *Cell*, 58: 15-25.

981 ———. 1991. 'Stepwise assembly of chromatin during DNA replication in vitro', *The EMBO*
982 *Journal*, 10: 971-80.

983 Süveges, Dániel, Zoltán Gáspári, Gábor Tóth, and László Nyitray. 2009. 'Charged single α-
984 helix: A versatile protein structural motif', *Proteins: Structure, Function, and*
985 *Bioinformatics*, 74: 905-16.

986 Swanson, Carter J., and Sivaraj Sivaramakrishnan. 2014. 'Harnessing the Unique Structural
987 Properties of Isolated α-Helices*', *Journal of Biological Chemistry*, 289: 25460-67.

988 Telmer, Patrick G., and Brian H. Shilton. 2003. 'Insights into the conformational equilibria of
989 maltose-binding protein by analysis of high affinity mutants', *The Journal of biological*
990 *chemistry*, 278: 34555-67.

991 Thomas, B. J., and R. Rothstein. 1989. 'The genetic control of direct-repeat recombination in
992 Saccharomyces: the effect of rad52 and rad1 on mitotic recombination at GAL10, a
993 transcriptionally regulated gene', *Genetics*, 123: 725-38.

994 Tyler, Jessica K., Christopher R. Adams, Shaw-Ree Chen, Ryuji Kobayashi, Rohinton T.
995 Kamakaka, and James T. Kadonaga. 1999. 'The RCAF complex mediates chromatin
996 assembly during DNA replication and repair', *Nature*, 402: 555-60.

997 Wei, Yang, Aby A. Thyparambil, and Robert A. Latour. 2014. 'Protein helical structure
998 determination using CD spectroscopy for solutions with strong background absorbance
999 from 190 to 230nm', *Biochimica et Biophysica Acta (BBA) - Proteins and Proteomics*,
1000 1844: 2331-37.

1001 Wolberger, Cynthia. 2021. 'How structural biology transformed studies of transcription
1002 regulation', *Journal of Biological Chemistry*, 296.

1003 Wolny, Marcin, Matthew Batchelor, Gail J. Bartlett, Emily G. Baker, Marta Kurzawa, Peter J.
1004 Knight, Lorna Dougan, Derek N. Woolfson, Emanuele Paci, and Michelle Peckham.
1005 2017. 'Characterization of long and stable de novo single alpha-helix domains provides
1006 novel insight into their stability', *Scientific Reports*, 7: 44341.

1007 Wolny, Marcin, Matthew Batchelor, Peter J. Knight, Emanuele Paci, Lorna Dougan, and
1008 Michelle Peckham. 2014. 'Stable Single α-Helices Are Constant Force Springs in
1009 Proteins', *Journal of Biological Chemistry*, 289: 27825-35.

1010 Woody, Robert W. 1996. 'Theory of Circular Dichroism of Proteins.' in Gerald D. Fasman (ed.),
1011 *Circular Dichroism and the Conformational Analysis of Biomolecules* (Springer US:
1012 Boston, MA).

1013 Yadav, Tejas, Jean-Pierre Quivy, and Geneviève Almouzni. 2018. 'Chromatin plasticity: A
1014 versatile landscape that underlies cell fate and identity', *Science*, 361: 1332-36.

1015 Ye, Xiaofen, Alexa A. Franco, Hidelita Santos, David M. Nelson, Paul D. Kaufman, and Peter D.
1016 Adams. 2003. 'Defective S phase chromatin assembly causes DNA damage, activation
1017 of the S phase checkpoint, and S phase arrest', *Molecular Cell*, 11: 341-51.

1018 Zhang, Kuo, Yuan Gao, Jingjing Li, Rebecca Burgess, Junhong Han, Huanhuan Liang, Zhiguo
1019 Zhang, and Yingfang Liu. 2016. 'A DNA binding winged helix domain in CAF-1 functions
1020 with PCNA to stabilize CAF-1 at replication forks', *Nucleic Acids Research*, 44: 5083-94.
1021
1022

Supplementary Information

Supplementary Table 1. List of plasmids.

Plasmid	Description	Reference
Cac1, pDONR/Zeo	Cac1 with C-terminal StrepII tag	(Liu et al., 2012)
Cac1 ΔKER, pDONR/Zeo	Cac1 without residues 136–225 and with C-terminal StrepII tag	This study
Cac1 ΔWHD, pDONR/Zeo	Cac1 without residues 520–606 and with C-terminal StrepII tag	This study
Cac1 Δmiddle-A, pDONR/Zeo	Cac1 without residues 155–204 and with C-terminal StrepII tag	This study
Cac1 ED::GSL, pDONR/Zeo	Cac1 residues 397–431 were replaced with glycine/serine/leucine linker. Contains C-terminal StrepII tag	This study
Cac1 +N-half, pDONR/Zeo	Cac1 residues 136–172 were introduced after the endogenous 225 residue of Cac1. Contains C-terminal StrepII tag	This study
Cac1 2xKER, pDONR/Zeo	Cac1 residues 136–225 were introduced after the endogenous 225 residue in Cac1. Contains C-terminal StrepII tag	This study
Cac1 KER::myosin7aSAH, pDONR/Zeo	Cac1 residues 136–225 were replaced with mouse Myosin 7a residues 866–932. Contains a C-terminal StrepII tag	This study
Cac1 KER::hKER, pDONR/Zeo	Cac1 residues 136–225 were replaced with CHAF1A residues 331–441. Contains a C-terminal StrepII tag	This study
Cac1, pDEST8	Cac1 with C-terminal StrepII tag	This study
Cac1 ΔKER, pDEST8	Cac1 without residues 136–225 and with C-terminal StrepII tag	This study
Cac1 ΔWHD, pDEST8	Cac1 without residues 520–606 and with C-terminal StrepII tag	This study
Cac1 Δmiddle-A, pDEST8	Cac1 without residues 155–204 and with C-terminal StrepII tag	This study
Cac1 ED::GSL, pDEST8	Cac1 residues 397–431 were replaced with glycine/serine/leucine linker. Contains C-terminal StrepII tag	This study
Cac1 +N-half, pDEST8	Cac1 residues 136–172 were introduced after the endogenous 225 residue of Cac1. Contains C-terminal StrepII tag	This study
Cac1 2xKER, pDONR/Zeo	Cac1 residues 136–225 were introduced after the endogenous 225 residue in Cac1. Contains C-terminal StrepII tag	This study
Cac1 KER::myosin7aSAH, pDEST8	Cac1 residues 136–225 were replaced with mouse Myosin 7a residues 866–932. Contains a C-terminal StrepII tag	This study
Cac1 KER::hKER, pDEST8	Cac1 residues 136–225 were replaced with hCHAF1A residues 331–441. Contains a C-terminal StrepII tag	This study

Cac2, pDONR/Zeo	Cac2 with C-terminal StrepII tag	This study
Cac2, pDEST8	Cac2 with C-terminal StrepII tag	This study
Cac3, pDONR/Zeo	Cac3 with C-terminal 3xFLAG tag	This study
Cac3, pDEST8	Cac3 with C-terminal 3xFLAG tag	This study
Cac1 KER, pDONR/Zeo	Cac1 residues 136–225	This study
Cac1 KER, pDEST566	Cac1 residues 136–225	This study
Cac1 KER, pDONR/Zeo	Cac1 residues 136–225 with C-terminal tyrosine	This study
Cac1 KER, pDEST566	Cac1 residues 136–225 with C-terminal tyrosine	This study
Cac1 N-half, pDONR/Zeo	Cac1 residues 136–172 with C-terminal tyrosine	This study
Cac1 N-half, pDEST566	Cac1 residues 136–172 with C-terminal tyrosine	This study
Cac1 C-half, pDONR/Zeo	Cac1 residues 179–225 with C-terminal tyrosine	This study
Cac1 C-half, pDEST566	Cac1 residues 179–225 with C-terminal tyrosine	This study
Cac1 middle-A, pDONR/Zeo	Cac1 residues 155–204 with C-terminal tyrosine	This study
Cac1 middle-A, pDEST566	Cac1 residues 155–204 with C-terminal tyrosine	This study
Cac1 middle-B, pDONR/Zeo	Cac1 residues 173–204 with C-terminal tyrosine	This study
Cac1 middle-B, pDEST566	Cac1 residues 173–204 with C-terminal tyrosine	This study
CHAF1A KER (hKER), pDONR/Zeo	CHAF1A residues 331–441 with C-terminal tyrosine	This study
CHAF1A KER (hKER), pDEST566	CHAF1A residues 331–441 with C-terminal tyrosine	This study
Myosin 7a SAH, pDONR/Zeo	Myosin 7a residues 866–932 with C-terminal tyrosine	This study
Myosin 7a SAH, pDEST566	Myosin 7a residues 866–932 with C-terminal tyrosine	This study
Cac1 WHD, pGEX-6P-1	Cac1 residues 457–606	(Liu et al., 2016)
CHAF1A, pGEX-6P-1	Human CHAF1A	This study

1027

Supplementary Table 2. List of synthetic DNA oligonucleotides and primers.

Name	Sequence (5'-3')
Cy5 601 10 nts. Sense	Cy5-CGCGCTGTCC
Cy5 601 20 nts. Sense	Cy5-ACGTACGCGCTGTCCCCCGC
Cy5 601 30 nts. Sense	Cy5-AACGCACGTACGCGCTGTCCCCCGCGTTTT
Cy5 601 40 nts. Sense	Cy5-GCTTAAACGCACGTACGCGCTGTCCCCCGCGTTTTAACCG
601 40 nts. Sense	GCTTAAACGCACGTACGCGCTGTCCCCCGCGTTTTAACCG
Cy5 601 50 nts. Sense	Cy5-GCACCGCTTAAACGCACGTACGCGCTGTCCCCCGCGTTTTAACCGCCAAG
Cy5 601 80 nts. Sense	Cy5-GTCGTAGACAGCTCTAGCACCGCTTAAACGCACGTACGCGCTGTCCCCCGCGTTTTAACCGCCAAGGGGATTACTCCCTA
601 10 nts. Antisense	GGACAGCGCG
601 20 nts. Antisense	GCGGGGGACAGCGCGTACGT
601 30 nts. Antisense	AAAACGCGGGGGACAGCGCGTACGTGCGTT
601 40 nts. Antisense	CGGTTAAAACGCGGGGGACAGCGCGTACGTGCGTTTAAGC
601 50 nts. Antisense	CTTGGCGGTTAAAACGCGGGGGACAGCGCGTACGTGCGTTTAAGCGGTGC
601 80 nts. Antisense	TAGGGAGTAATCCCCTTGGCGGTTAAAACGCGGGGGACAGCGCGTACGTGCGTTTAAGCGGTGCTAGAGCTGTCTACGAC
Cac1 ΔKER Forward	GCACAATCCCGTATTGGTAACTTCTTTAAAAAACTAAGCG
Cac1 ΔKER Reverse	TTACCAATACGGGATTGTGCCGATGAGGAAAGTTCTCTCTTAGAGCATGG
Cac1 Δmiddle-A Forward	AGAAAAGAGGAGGAAAGATTGAAAAAGGAGGAGGAAATACG
Cac1 Δmiddle-A Reverse	AATCTTTCCTCCTCTTTTCTTTTCTCTTCTGCACGTTGCTGCTTTTTTAGTTCC
Cac1 ΔWHD Forward	ATGCCAACCCCGTCTTTGTCAGGATGGAGCCACCCGCAGTTCGAAAAGTAG
Cac1 ΔWHD Reverse	GACAAAGACGGGGTTGGCATTTTCTTTTCGGGACTTTGAGATTGGCTAGCGG
Cac1 KER::Myosin7a SAH Forward	GCACAATCCCGTATTGGTAA
Cac1 KER::Myosin7a SAH Reverse	CGATGAGGAAAGTTCTCTCT
Cac1 KER::Myosin7a SAH dsDNA	AGAGAGAACTTTCCTCATCGCGCCTGGAAGCGGAACGCATGCGCCTGGCGGAAGAAGAAAAACTGCGCAAAGAAATGAGCGCGAAAAAAGCGAAAGAAGAAGCGGAACGCAAACATCAGGAACGCCTGGCGCAGCTGGCGCGCGAAGATGCGGAACGCGAACTGAAAGAAAAAGAAGAAGCGCGCCGCAAAAAAGAACTGCTGGAACAGATGGAAAAAGCGGCACAATCCCGTATTGGTAA
Cac1 ED::GSL Forward	AACAGTGATTTGGATGGCCTACCCTGC

Cac1 ED::GSL Reverse	TTCTTCTTCTTCATTAACCCATTCAACG
Cac1 ED::GSL dsDNA	GGGTTAATGAAGAAGAAGAAGGCTCACTGGGGTCCCTT GGAAGCTTAGGGTCTCTTGGGTCCCTGGGCTCTTTAGG AAGCCTTGGTTCACTTGGTTCATTAGGATCCCTAGGATC TTTGGGATCCAACAGTGATTTGGATGGCCT
Cac1 2xKER Forward	GCACAATCCCGTATTGGTAA
Cac1 2xKER Reverse	TCTTTCCTTGGCTTCTTCTTTCAAACG
Cac1 2xKER dsDNA -Fwd	AAGAAGAAGCCAAGGAAAGAAAAAAGGAAGAAGCTAAAA GAGAAAAGG
Cac1 2xKER dsDNA -Rev	TTACCAATACGGGATTGTGCTCTTTCCTTGGCTTCTTCTT TCAAACGTATTTCCTCC
Cac1 +N-half Forward	GCACAATCCCGTATTGGTAA
Cac1 +N-half Reverse	TCTTTCCTTGGCTTCTTCTTTCAAACG
Cac1 +N-half dsDNA	AAGAAGAAGCCAAGGAAAGAAAAAAGGAAGAAGCTAAAA GAGAAAAGGAACTAAAAAAGCAGCAACGTGCAGAAGAG AAACACAGAAAAGAGTTATTACGACAAGAAGAGAAAAAG AAAAAAGAGCTAAAGGCACAATCCCGTATTGGTAA
Cac1 KER::hKER Forward	GCACAATCCCGTATTGGTAA
Cac1 KER::hKER Reverse	CGATGAGGAAAGTTCTCTCT
Cac1 KER::hKER dsDNA -Fwd	AGAGAGAACTTTCCTCATCGGAAAAGAACAAACTGCGCC TGCAACGCGACC
Cac1 KER::hKER dsDNA -Rev	TTACCAATACGGGATTGTGCTTCCGCTTTGATACGCTTTT CTTC
Cac1 KER Forward	CTGTTCCAGGGGCCCCTGAAAAAGGAAGAAGCTAAAAG AGAAAAGG
Cac1 KER Reverse	GGGGACCACTTTGTACAAGAAAGCTGGGTCCTACTATCT TTCCTTGGCTTCTTCTTTC
Cac1 KER Reverse +Y	GGGGACCACTTTGTACAAGAAAGCTGGGTCCTACTAATA TCTTTCCTTGGCTTCTTCTTT
Cac1 N-half Forward	CTGTTCCAGGGGCCCCTGAAAAAGGAAGAAGCTAAAAG AGAAAAGG
Cac1 N-half Reverse	GGGGACCACTTTGTACAAGAAAGCTGGGTCCTACTAATA CTTTAGCTCTTTTTTCTTTTT
Cac1 middle-A dsDNA	GGGGACAAGTTTGTACAAAAAAGCAGGCTTCCTGGAAGT TCTGTTCCAGGGGCCCCTGAAACATCGTAAAGAATTACT TCGTCAAGAAGAAAAGAAAAAGAAGGAACTTAAAGTAGA GGAAGAACGGCAGCGGCGGGCTGAACTGAAAAAGCAG AAGGAAGAGGAAAAACGGCGTAAAGAGGAGGCGCGTTT GGAGGCCAAACGGCGCTAT TAGTAGGACCCAGCTTTCTTGTACAAAGTGGTCCCC
Cac1 middle-B dsDNA	GGGGACAAGTTTGTACAAAAAAGCAGGCTTCCTGGAAGT TCTGTTCCAGGGGCCCCTGGTAGAGGAAGAACGGCAGC GGCGGGCTGAACTGAAAAAGCAGAAGGAAGAGGAAAAA CGGCGTAAAGAGGAGGCGCGTTTGGAGGCCAAACGGC GCTATTAGTAGGACCCAGCTTTCTTGTACAAAGTGGTCC CC
Cac1 C-half Forward	CTGTTCCAGGGGCCCCTGAGGCGTGCTGAGCTGAAAAA GC

Cac1 C-half Reverse	GGGGACCACTTTGTACAAGAAAGCTGGGTCCTACTAATA CTCTTTTCTTCTTTT GGC
Myosin 7a SAH dsDNA	GGGGACAAGTTTGTACAAAAAAGCAGGCTTCCTGGAAGT TCTGTTCCAGGGGCCCCTGCGCCTGGAAGCGGAACGCA TGCGCCTGGCGGAAGAAGAAAAACTGCGCAAAGAAATG AGCGCGAAAAAAGCGAAAGAAGAAGCGGAACGCAAACA TCAGGAACGCCTGGCGCAGCTGGCGCGCGAAGATGCG GAACGCGAACTGAAAGAAAAAGAAGAAGCGCGCCGCAA AAAAGAACTGCTGGAACAGATGGAAAAAGCG TATTAGTAGGACCCAGCTTTCTTGTACAAAGTGGTCCCC
CHAF1A dsDNA for cloning in pGEX-6P-1	GGGGCCCCTGGGATCCATGGATTGCAAAGATCGCCCGG CGTTTCCGGTGAAAAAACTGATTCAGGCGCGCCTGCCG TTCAAGCGCCTGAACCTGGTGCCGAAAGGCAAAGCGGA TGATATGAGCGACGATCAAGGTACGAGCGTTCAGAGCA AATCGCCGGATCTGGAAGCCAGCCTGGATACGCTGGAA AACAACTGTCACGTGGGTAGCGATATTGACTTTCGCCCG AAACTGGTTAATGGTAAAGGCCCGCTGGATAATTTTCTG CGCAACCGCATTGAAACCAGCATCGGCCAGAGCACCGT TATCATTGATCTGACCGAGGATAGCAACGAGCAGCCGG ATAGCCTGGTGGATCATAACAAACTGAACAGCGAGGCG AGCCCGTCGCGCGAGGCGATCAATGGCCAGCGCGAAG ACACCGGTGATCAACAGGGTTTACTGAAGGCGATTCAAA ATGACAAACTGGCCTTCCCGGGTGAAACCCTGAGCGAC ATTCCGTGTAAGACCGAGGAAGAAGGTGTGGGTTGTGG TGGCGCGGGCCGCCGTGGCGATAGCCAGGAATGCAGC CCGCGCAGCTGTCCGGAACTGACGAGCGGTCCGCGCA TGTGTCCGCGCAAGGAACAAGATAGCTGGAGCGAGGCC GGCGGCATTCTGTTCAAGGGAAAAGTTCCGATGGTTGTT CTGCAGGACATTCTGGCGGTGCGCCCTCCGCAGATCAA AAGCCTGCCGGCCACGCCGCAAGGCAAAAACATGACGC CGGAAAGCGAAGTGCTGGAAAGCTTTCCGGAAGAGGAC AGCGTTCTGAGCCATTCGAGCCTGTCGAGCCCGAGCAG CACCTCGAGCCCGGAAGGTCCTCCGGCCCCGCCGAAG CAGCATTCGAGCACGAGCCCGTTTCCGACGAGCACCCC GCTGCGTCGCATTACCAAGAAATTTGTGAAAGGTAGCAC GGAAAAGAACAAACTGCGCCTGCAACGCGACCAAGAAC GCCTGGGTAAGCAACTGAAACTGCGCGCCGAGCGCGA GGAAAAGGAAAAGCTGAAAGAGGAAGCCAAACGCGCCA AGGAGGAGGCGAAGAAAAAAAAGGAGGAAGAAAAGGAA CTGAAGGAGAAAGAGCGCCGTGAAAAGCGCGAAAAGGA TGAGAAGGAAAAAGCGGAAAAACAACGCCTGAAGGAGG AACGCCGTAAAGAACGCCAGGAAGCCCTGGAAGCCAAA CTGGAAGAAAAACGCAAAAAGGAGGAAGAAAAGCGTCT GCGCGAGGAAGAAAAGCGTATCAAAGCGGAAAAGGCGG AAATTACCCGCTTCTTCCAGAAGCCGAAGACGCCTCAGG CCCCGAAGACGCTGGCGGGTAGCTGTGGTAAATTTGCC CCGTTCGAGATTAAGGAACATATGGTGCTGGCCCCGCG TCGCCGCACGGCGTTTCATCCGGACCTGTGCAGCCAGC TGGACCAGCTGCTGCAGCAGCAGAGCGGTGAGTTCTCG TTCCTGAAGGATTTAAAGGGCCGCCAACCGCTGCGCAG CGGTCCGACCCACGTTAGCACGCGCAACGCCGATATCT

	TCAATAGCGACGTTGTGATCGTGGAGCGCGGCAAAGGC
	GACGGTGTTCCGGAGCGTCGCAAGTTTGGACGCATGAA
	GTTACTGCAATTCTGCGAGAACCATCGCCCGGCCTATTG
	GGGCACGTGGAACAAGAAAACTGCGCTGATTCGCGCGC
	GTGATCCGTGGGCCCAGGATACGAAGTTACTGGACTAC
	GAAGTTGATAGCGATGAAGAGTGGGAAGAAGAGGAACC
	GGGTGAGAGCCTGTCGCACAGCGAGGGCGACGATGAT
	GACGACATGGGTGAGGATGAGGACGAAGACGATGGTTT
	CTTTGTGCCTCATGGTTACCTGAGCGAAGACGAGGGTG
	TTACCGAAGAGTGTGCGGACCCGGAAAACCATAAGGTG
	CGCCAGAAGCTGAAGGCCAAAGAGTGGGACGAGTTCCT
	GGCGAAGGGCAAACGTTTTCGCGTTCTGCAGCCGGTTA
	AAATTGGCTGTGTTTGGGCCGCGGATCGCGACTGCGCG
	GGTGATGACCTGAAAGTTCTGCAGCAATTCGCGGCCTG
	CTTCCTGGAGACCCTGCCGGCGCAGGAGGAACAAACCC
	CGAAAGCCAGCAAACGCGAACGTCGCGATGAGCAGATT
	CTGGCGCAGTTACTGCCGTTACTGCATGGCAACGTTAAC
	GGTAGCAAAGTGATCATTCGCGAATTCCAGGAGCACTG
	CCGTCGCGGTTTACTGAGCAATCATACCGGTAGCCCGC
	GCACGCCGAGCACCACCTACCTGCATACGCCGACCCCG
	AGCGAGGATGCCGCGATTCCGAGCAAGTCGCGCCTGAA
	GCGCCTGATTAGCGAAAATAGCGTTTACGAAAAGCGCC
	CGGACTTTCGCATGTGTTGGTACGTGCATCCGCAGGTG
	CTGCAGAGCTTTCAGCAGGAACATCTGCCGGTTCCGTG
	CCAATGGAGCTACGTTACGAGCGTGCCGAGCGCCCCGA
	AAGAGGATAGCGGTAGCGTGCCGAGCACGGGTCCGAG
	CCAAGGTACCCCGATCAGCCTGAAGCGCAAGAGCGCCG
	GTAGCATGTGCATTACCCAATTTATGAAGAAACGTCGCC
	ATGACGGCCAGATCGGTGCGGAGGACATGGACGGTTTT
	CAAGCGGATACCGAGGAAGAGGAAGAAGAAGAGGGCG
	ACTGCATGATTGTTGATGTTCCGGACGCCGTGGAAGTTC
	AGGCCCCGTGTGGTGCCGCGAGCGGGGCCGGTGGCG
	GCGTTGGCGTGGATACCGGAAAAGCGACCCTGACGGCC
	AGCCCGCTGGGTGCGAGCTAAGGATCCCCGGAATTCC
CHAF1A KER (hKER) Forward	GGGGACAAGTTTGTACAAAAAAGCAGGCTTCCTGGAAGT TCTGTTCCAGGGGCCCCTGGAAAAGAACAAACTGCGCC TGCAACGCGACC
CHAF1A KER (hKER) Reverse	GGGGACCACTTTGTACAAGAAAGCTGGGTCCTACTAATA TTCCGCTTTGATACGCTTTTCTTC
CAC1_FLAG_gRNA_F	CTTTCCGTTCAAGTTACAAAGACG
CAC1_FLAG_gRNA_R	AAACCGTCTTTGTAACTTGAACGG
mPIP_Δ225-226_gRNA_F	CTTTACGTTTGAAAGAAGAAGCCA
mPIP_Δ225-226_gRNA_R	AAACTGGCTTCTTCTTTCAAACGT
mWHD_gRNA_F	CTTTAACAATTAAAAACACCATAA
mWHD_gRNA_R	AAACTTATGGTGTTTTTAATTGTT
ΔKER_gRNA_F	CTTTAGGTAGAAGAGGAAAGACAA
ΔKER_gRNA_F	AAACTTGTCTTTCCTCTTCTACCT
Δ145-149_gRNA_R	CTTTGGAAGAAGCTAAAAGAGAAA
Δ145-149_gRNA_R	TTTCTCTTTTAGCTTCTTCC

CAC1_FLAG_HR_F	CCAATGCAAATATGCCAACCCCGTCTTTGGGATCCGCTG GCTCCGCTGCTGGTTCTGGCG
CAC1_FLAG_HR_M	GGTTCTGGCGATTACAAGGATGACGACGATAAGGACTAT AAGGACGATGATGACAAGGACTACAAAGATGATGACGAT AAATAACTTGAA
CAC1_FLAG_HR_R	TACCAATAAATAATCAGTTTATCTGTATGTTTCTATATACT AAAGATCCGTTCAAGTTAT
CAC1_mPIP_HR_F	AAATACGTTTGAAAGAAGAAGCCAAAGAAAGAGCACAAT CCCGTATTGGTAACGC
CAC1_mPIP_HR_M	TTGGTAACGCCGCGAAAAAACTAAGCGATTCTAATACGC CTGTGGTTGAAAAGTCGGATT
CAC1_mPIP_HR_R	CTCTAACTCCATCTTTAGCATAGAAAGGTAGAAAAAATTT TTCATAATCCGACTT
CAC1_mWHD_HR_F	CAGCACGTTTTCTTTGGGTACTGTGACTGAAATAGCACA GAAAAATTTGCCGCAATACAA
CAC1_mWHD_HR_M	CGCAATACAACAAACAAACAATTGAAAACACCATAGAGG AATATGCCATAAGAAGTTCTG
CAC1_mWHD_HR_R	CCAGTTTTGTGCGTCTTTGATTACCCATTTGCGGGGCAA ATCACCCTTTCCAGAACTTCT
CAC1_ΔKER_HR_F	TACCCAATGGAAATATAATAGCTATCGAGACAAAAAGCA GAAGCTCTTCTCCATGCTCTA
CAC1_ΔKER_HR_M	TCTCCATGCTCTAAGAGAGAACTTTCCTCATCGGCACAA TCCCGTATTGGTAACTTCTTT
CAC1_ΔKER_HR_R	TCATAATCCGACTTTTCAACCACAGGCGTATTAGAATCG CTTAGTTTTTTAAAGAAGTTA
CAC1_ΔKERmPIP_HR_M	TCTCCATGCTCTAAGAGAGAACTTTCCTCATCGGCACAA TCCCGTATTGGTAACGCCGCG
CAC1_ΔKERmPIP_HR_R	TCATAATCCGACTTTTCAACCACAGGCGTATTAGAATCG CTTAGTTTTTTCGCGGCGTTA
CAC1_Δ1-2KER_HR_F	CTAAGAGAGAACTTTCCTCATCGAAAAAGGAAGAAGCTA AAAGAGAAAAGGAACTAAAAA
CAC1_Δ1-2KER_HR_M	GAACTAAAAAAGCAGCAACGTGCAGAAGAGAAAGAGGA GGAAAGATTGAAAAAGGAGGAG
CAC1_Δ1-2KER_HR_R	CCAATACGGGATTGTGCTCTTTCCTTGGCTTCTTCTTTCA AACGTATTTCCTCCTCCTTT
CAC1_2xandHumanKER_ HR_F	GCTATCGAGACAAAAAGCAGAAGCTCTTCTCCATGCTCT AAGAGAGAACTTTCCTCATCG
CAC1_2xandHumanKER_ HR_R	AACCACAGGCGTATTAGAATCGCTTAGTTTTTTAAAGAAG TTACCAATACGGGATTGTGC
CAC1_Δ225-226_HR_F	GATTAGAAGCCAAAAGAAGAAAAGAGGAGGAAAGATTGA AAAAGGAAGAGGAAATACGTT
CAC1_Δ225-22_HR_M	GAAATACGTTTGAAAGAAGAAGCCAAAGAACAATCCCGT ATTGGTAACTTCTTTAAAAAA
CAC1_Δ225-226_HR_R	AATTTTTCATAATCCGACTTTTCAACCACAGGCGTATTAG AATCGCTTAGTTTTTTAAAG
CAC1_Δ225-226mPIP_HR_M	GAAATACGTTTGAAAGAAGAAGCCAAAGAACAATCCCGT ATTGGTAACGCCGCGAAAAAA
CAC1_Δ225-226mPIP_HR_R	AATTTTTCATAATCCGACTTTTCAACCACAGGCGTATTAG AATCGCTTAGTTTTTTCGCG
CAC1_Δ145-149_HR_F	AAAAGCAGAAGCTCTTCTCCATGCTCTAAGAGAGAACTT TCCTCATCGAAAAAGGAAGAA

CAC1_Δ145-149_HR_M	AAAGGAAGAAGCTAAAAGAGAAAAGCAACGTGCAGAAG AGAAACACAGAA
CAC1_Δ145-149_HR_R	TTCTACCTTTAGCTCTTTTTTCTTTTTCTCTTCTTGTCGTA ATAACTCTTTTCTGTGTTT
Yeast::Human KER	AAGAGAGAACTTTCCTCATCGGAAAAAAATAAGCTGAGA TTACAACGTGACCAAGAGAGGCTGGGAAAGCAACTTAAA CTTAGAGCCGAGCGTGAAGAAAAGGAGAAGCTAAAAGA AGAAGCTAAGAGGGCTAAGGAAGAGGCTAAAAAAAAGA AAGAAGAAGAGAAAGAGTTGAAAGAGAAAGAAAGGAGG GAAAAACGTGAAAAGGATGAAAAGGAGAAGGCAGAAAA GCAGCGTTTAAAAGAAGAGAGAAGAAAGGAACGTCAAG AAGCATTAGAAGCAAAGCTGGAGGAAAAGAGGAAGAAA GAAGAGGAAAAGAGGTTACGTGAAGAAGAAAAAAGAATA AAGGCTGAGGCACAATCCCGTATTGGTAAC
2xKER	AAGAGAGAACTTTCCTCATCGAAAAAAGAAGAAGCAAAG AGGGAAAAGGAGCTTAAAAAGCAACAACGTGCTGAAGA GAAGCATAGGAAAGAATTGTTGAGACAGGAAGAAAAAAA GAAGAAAGAACTGAAGGTGGAGGAAGAGAGACAAAGGA GGGCCGAACTAAAAAAGCAGAAGGAGGAGGAAAAACGT CGTAAAGAAGAGGCGAGACTAGAGGCGAAAAGGAGAAA AGAAGAAGAAAGGTTGAAAAAGGAGGAGGAAATTAGGTT AAAAGAAGAAGCGAAGGAAAGGAAAAAGGAGGAGGCAA AGCGTGAGAAGGAGCTAAAGAAACAGCAACGTGCAGAA GAGAAACACAGAAAGGAGTTGTTGAGGCAGGAAGAAAA AAAAAAAAAGGAACTAAAAGTCGAAGAAGAAAGACAGAG ACGTGCCGAACTAAAAAAACAAAAAGAAGAAGAGAAGCG TAGAAAGGAAGAAGCAAGGCTTGAAGCAAAACGTAGGA AGGAAGAGGAACGTCTGAAGAAAGAGGAGGAGATCAGA CTAAAGGAAGAGGCTAAAGAGAGAGCACAATCCCGTATT GGTAAC
rtt106_HIS_F	TGTAGTAATAACTATGATGTAAAGGTGCTGGAAACGCTG ACAGCTGAAGCTTCGTACGC
rtt106_HIS_R	TATTCTTCAGGATAAAAAAAGTGGTATTTATGAACTCTTA CATAGGCCACTAGTGGATCTG
cac1_KAN_F	ACATTCTGTTATTGCTGTTACAGAGAATTATATGTTTTAG CAGCTGAAGCTTCGTACGC
cac1_KAN_R	TAGTGTTGTCGCCTTTTTCATGTATACCAATAAATAATCA CATAGGCCACTAGTGGATCTG
sir2_KAN_F	CCCATCTCAGAGAAAAAACGAGG
sir2_KAN_R	AGCTATTTGTGAGAGCCTTGCGTC
bar1_LEU2_F	GCCAGCTATTCTGAAACACACCAC
bar1_LEU2_R	GCTACTTGTTCAAAATTGTGATGGCTGC
bar1_LEU2_R	GCTACTTGTTCAAAATTGTGATGGCTGC

1030

1031 **Supplementary Table 3.** List of yeast strains.
1032

Strain	Mutation	Genotype	Reference
W303-1a		*Mat a ade2-1 leu2-2,112 his3-11,15 trp1 ura3-1 can1-100*	(Thomas and Rothstein, 1989)
RAY160	rtt106Δ	*Mat a ade2-1 leu2-2,112 his3-11,15 trp1 ura3-1 can1-100 rtt106::HIS3*	This study
RAY165	rtt106Δcac1Δ	*Mat a ade2-1 leu2-2,112 his3-11,15 trp1 ura3-1 can1-100 rtt106::HIS3 cac1::KANMX*	This study
RAY187	mPIP	RAY160 *CAC1 F233A/F234A*	This study
RAY180	mWHD	RAY160 *CAC1 K564E/K568E*	This study
RAY192	mPIP + mWHD	RAY160 *CAC1 F233A/F234A/K564E/K568E*	This study
RAY264	ΔKER)	RAY160 *CAC1 Δ136-225*	This study
RAY265	ΔKER + mPIP	RAY264 *CAC1 F233A/F234A*	This study
RAY266	ΔKER + mWHD	RAY264 *CAC1 K564E/K568E*	This study
RAY221	Δmiddle-AKER	RAY160 *CAC1 Δ155-204*	This study
RAY222	Δmiddle-AKER + mPIP	RAY221 *CAC1 F233A/F234A*	This study
RAY223	Δmiddle-AKER + mWHD	RAY221 *CAC1 K564E/K568E*	This study
RAY245	2xKER)	RAY160 *CAC1 dup(136-225)*	This study
RAY258	2xKER + mPIP	RAY245 *CAC1 F233A/F234A*	This study
RAY247	2xKER + mWHD	RAY245 *CAC1 K564E/K568E*	This study
RAY233	yeast KER::human KER	RAY160 *CAC1 136-225::hCHAF1A 331-441*	This study
RAY256	yeast KER::human KER + mPIP	RAY233 *CAC1 F233A/F234A*	This study
RAY243	yeast KER::human KER + mWHD	RAY233 *CAC1 K564E/K568E*	This study
RAY226	Δ225-226	RAY160 *CAC1 Δ225-226*	This study
RAY239	Δ225-226 + mPIP	RAY226 *CAC1 F223A/F234A*	This study
RAY241	Δ225-226 + mWHD	RAY226 *CAC1 K564E/K568E*	This study
RAY207	Δ145-149	RAY160 *CAC1 Δ145-149*	This study
RAY216	Δ145-149 + mPIP	RAY207 *CAC1 F233A/F234A*	This study
RAY218	Δ145-149 + mWHD	RAY207 *CAC1 K564E/K568E*	This study
BY4741		*Mat a his3Δ1 leu2Δ0 met15Δ0 ura3Δ0*	(Baker Brachmann et al., 1998)
[a]RAY156		*Mat a his3Δ1 leu2Δ0 met15Δ0 ura3Δ0 hmr::P_{URA3}-GFP/URA3 TRP::BrdU-Inc(TRP) bar1::LEU2*	This study
[a]RAY152	*sir2Δ*	*Mat a his3Δ1 leu2Δ0 met15Δ0 ura3Δ0 hmr::P_{URA3}-GFP/URA3 TRP::BrdU-Inc(TRP) sir2::KANMX*	This study

[a]RAY177	*rtt106Δ*	*Mat a his3Δ1 leu2Δ0 met15Δ0 ura3Δ0 hmr::P_{URA3}-GFP/URA3 TRP::BrdU-Inc(TRP) bar1::LEU2 rtt106::HIS3*	This study
[a]RAY179	*cac1Δ*	*Mat a his3Δ1 leu2Δ0 met15Δ0 ura3Δ0 hmr::P_{URA3}-GFP/URA3 TRP::BrdU-Inc(TRP) bar1::LEU2 cac1::KANMX*	This study
[a]RAY189	*rtt106Δcac1Δ*	*Mat a his3Δ1 leu2Δ0 met15Δ0 ura3Δ0 hmr::P_{URA3}-GFP/URA3 TRP::BrdU-Inc(TRP) bar1::LEU2 rtt106::HIS3 cac1::KANMX*	This study
RAY193	mPIP	RAY177 *CAC1 F233A/F234A*	This study
RAY194	mWHD	RAY177 *CAC1 K564E/K568E*	This study
RAY199	mPIP + mWHD	RAY177 *CAC1 F233A/F234A/K564E/K568E*	This study
RAY205	ΔKER	RAY177 *CAC1 Δ136-225*	This study
RAY212	ΔKER + mPIP	RAY205 *CAC1 F233A/F234A*	This study
RAY206	ΔKER + mWHD	RAY205 *CAC1 K564E/K568E*	This study
RAY219	Δmiddle-A	RAY177 *CAC1 Δ155-204*	This study
RAY259	Δmiddle-A + mPIP	RAY219 *CAC1 F233A/F234A*	This study
RAY230	Δmiddle-A + mWHD	RAY219 *CAC1 K564E/K568E*	This study
RAY244	2xKER	RAY177 *CAC1 dup(136-225)*	This study
RAY263	2xKER + mPIP	RAY244 *CAC1 F233A/F234A*	This study
RAY246	2xKER + mWHD	RAY244 *CAC1 K564E/K568E*	This study
RAY232	yeast KER::human KER	RAY177 *CAC1 136-225::hCHAF1A 331-441*	This study
RAY257	yeast KER::human KER + mPIP	RAY232 *CAC1 F233A/F234A*	This study
RAY242	yeast KER::human KER + mWHD	RAY232 *CAC1 K564E/K568E*	This study
RAY225	Δ225-226	RAY177 *CAC1 Δ225-226*	This study
RAY238	Δ225-226 + mPIP	RAY225 *CAC1 F223A/F234A*	This study
RAY240	Δ225-226 + mWHD	RAY225 *CAC1 K564E/K568E*	This study
RAY208	Δ145-149	RAY177 *CAC1 Δ145-149*	This study
RAY209	Δ145-149 + mPIP	RAY208 *CAC1 F233A/F234A*	This study
RAY231	Δ145-149 + mWHD	RAY208 *CAC1 K564E/K568E*	This study
RAY191	CAC1-FLAG	*Mat a ade2-1 leu2-2,112 his3-11,15 trp1 ura3-1 can1-100 rtt106::HIS3 CAC1-3xFLAG*	This study
RAY195	CAC1-FLAG mPIP	RAY191 *CAC1 F233A/F234A*	This study
RAY196	CAC1-FLAG mWHD	RAY191 *CAC1 K564E/K568E*	This study

RAY197	CAC1-FLAG mPIP + mWHD	RAY191 *CAC1 F233A/F234A/K564E/K568E*	This study
RAY203	CAC1-FLAG ΔKER	RAY191 *CAC1 Δ136-225*	This study
RAY214	CAC1-FLAG ΔKER + mPIP	RAY214 *CAC1 F233A/F234A*	This study
RAY207	CAC1-FLAG ΔKER + mWHD	RAY214 *CAC1 K564E/K568E*	This study
RAY220	CAC1-FLAG Δmiddle-A	RAY191 *CAC1 Δ155-204*	This study
RAY250	CAC1-FLAG Δmiddle-A + mPIP	RAY250 *CAC1 F233A/F234A*	This study
RAY224	CAC1-FLAG Δmiddle-A + mWHD	RAY250 *CAC1 K564E/K568E*	This study
RAY254	CAC1-FLAG 2xKER	RAY191 *CAC1 dup(136-225)*	This study
RAY255	CAC1-FLAG 2xKER + mPIP	RAY254 *CAC1 F233A/F234A*	This study
RAY261	CAC1-FLAG 2xKER + mWHD	RAY254 *CAC1 K564E/K568E*	This study
RAY262	CAC1-FLAG yeast KER::human KER	RAY191 *CAC1 136-225::hCHAF1A 331-441*	This study
RAY260	CAC1-FLAG yeast KER::human KER + mPIP	RAY262 *CAC1 F233A/F234A*	This study
RAY253	CAC1-FLAG yeast KER::human KER + mWHD	RAY262 *CAC1 K564E/K568E*	This study
RAY229	CAC1-FLAG Δ225-226	RAY191 *CAC1 Δ225-226*	This study
RAY248	CAC1-FLAG Δ225-226 + mPIP	RAY248 *CAC1 F223A/F234A*	This study
RAY249	CAC1-FLAG Δ225-226 + mWHD	RAY229 *CAC1 K564E/K568E*	This study
RAY215	CAC1-FLAG Δ145-149	RAY191 *CAC1 Δ145-149*	This study
RAY251	CAC1-FLAG Δ145-149 + mPIP	RAY251 *CAC1 F233A/F234A*	This study
RAY217	CAC1-FLAG Δ145-149 + mWHD	RAY251 *CAC1 K564E/K568E*	This study

[a] *BrdU-Inc(*Viggiani and Aparicio, 2006*); hmr::PURA3-GFP/URA3(*Laney and Hochstrasser, 2003*).*

Supplementary Table 4. Statistics for crystallographic data collection and refinement.

Data statistics	MBP-KER (PDB: 8DEI)
Spacegroup	$P2_1$
Cell dimensions (Å)	a=53.586 b=165.249 c=116.149 α=90° β=96.47° γ=90°
Resolution range (Å)	26.68 - 2.81 (2.9? - 2.81)[a]
Total reflections	188,138 (13,259)[a]
Unique reflections	48320 (4400)[a]
Redundancy	3.9 (3.0)[a]
R_{sym}[b] (%)	17.6 (68.9)[a]
Completeness (%)	97.76 (90.08)[a]
Intensity (I/σ)	7.3 (???)[a]
CC1/2	.979 (695)
Wilson B factor (Å^2)	46.75
Refinement statistics	
Resolution Range (Å)	28.68 - 2.81 (2.91 - 2.81)[a]
Unique reflections	47,773 (4364)
Rfree[c] (%)	28.25 (35.43)[a]
Rworking (%)	23.30 (29.20)[a]
Final Model	
Number of protein atoms	14,659
Number of heteroatoms	106
Number of solvent atoms	11
Average B factor (Å^2)	51.56
R.m.s.d. bond lengths (Å)	0.001
R.m.s.d. bond angles (°)	0.342
Molprobity score	1.39
Ramachandran Analysis	96.44% most favored; 3.56% allowed; 0% outlier

[a] *High resolution shell*

[b] $R_{sym} = \Sigma|I - \langle I \rangle| / \Sigma I$

[c] R_{free} *calculated with an excluded set of 10%*

Supplementary References

Laney, Jeffrey D., and Mark Hochstrasser. 2003. 'Ubiquitin-dependent degradation of the yeast Matα2 repressor enables a switch in developmental state', *Genes and Development*, 17: 2259-70.

Viggiani, Christopher J., and Oscar M. Aparicio. 2006. 'New vectors for simplified construction of BrdU-Incorporating strains of Saccharomyces cerevisiae', *Yeast*, 23: 1045-51.

Source Data Files – Legends

Figure 1 - Source data 1. The yKER region favors binding to tetrasome-length DNA and facilitates the function of yCAF-1 *in vivo*. EMSA images (panels b, c, d and e) and data analyses (panel j).

Figure 1 - Source data 2. The yKER region favors binding to tetrasome-length DNA and facilitates the function of yCAF-1 *in vivo*. EMSA images (panels f, g, h, i and m), data analyses (panel k and l) and flow cytometry data (panel o).

Figure 1 - figure supplement 1 - Source data 1. Quality of proteins used in this study. SDS-PAGE (panels a-c) and Western blots (panel d)

Figure 1 - figure supplement 2 - Source data 1. CAF-1 DNA binding analysis and *in vivo* assays. EMSA images (panels a and b), data analyses (panel c) and flow cytometry data (panel f)

Figure 2 - Source data 1. The yKER is a single alpha-helix (SAH) domain that forms a stable complex with DNA. Circular dichroism data (panels c and d)

Figure 2 - figure supplement 1 - Source data 1. MBP-yKER oligomeric properties. EMSA images and data analyses (panels d and e)

Figure 2 - figure supplement 2 - Source data 1. DNA binding properties of the yKER. Circular dichroism data (panel a) and EMSA images (panel b)

Figure 3 - Source data 1. The yKER middle region is required for DNA binding and yCAF-1 function *in vivo*. Circular dichroism data (panel b), EMSA images (panels c-h), Flow cytometry data (panel j) and data analyses (panels c-f, j).

Figure 4 - Source data 1. The yKER confers DNA-length selectivity to yCAF-1. EMSA images and data analyses

Figure 5 - Source data 1. The length and the phase of the yKER SAH modulates yCAF-1 functions *in vivo*. EMSA images (panel a) and Flow cytometry data (panel c).

Figure 5 - figure supplement 1 - Source data 1. Analysis of the yKER length. EMSA images and data analyses (panel a)

Figure 6 - Source data 1. DNA-length selectivity by the KER is species specific and its function is not conserved *in vivo*. EMSA images and data analyses (panels b and c) and Flow cytometry data and analyses (panel e)

Figure 6 - figure supplement 1 - Source data 1. Analysis of the substitution of the yKER with the hKER. Circular dichroism data (panels b and c)